

A review of the role of subduction dynamics for regional and global plate motions

Thorsten W. Becker¹ and Claudio Faccenna²

¹Department of Earth Sciences, University of Southern California, 3651 Trousdale Parkway, Los Angeles CA90089-0740, USA. Email: twb@usc.edu

²Università di Roma TRE, Rome, Italy

In press at: *Subduction Zone Geodynamics* special volume, *Frontiers in Earth Sciences*, Lallemand, S. and Funicello, F., Eds., *Int. J. Earth Sci.*, revised version as of December 14, 2007; in original form on August 2, 2007.

Abstract

Subduction of oceanic lithosphere and deep slabs control several aspects of plate tectonics. We review models of subduction dynamics that have been studied over the last decade by means of numerical and analog experiments. Regional models indicate that trench rollback, trench curvature, and back-arc deformation may be explained by fluid slabs that are ~ 250 to 500 times stiffer than the upper mantle. Slab width and, more importantly, rheology determine the role of viscous bending, poloidal-sinking flow and toroidal-rollback stirring, and interactions of the slab with the higher viscosity lower mantle. Several of these contributions can be represented by a local sinking velocity. Back-arc deformation may then result from an imbalance if larger-scale plate forcing leads to deviations of the convergence rate from the local equilibrium. Lateral viscosity variations (LVVs) are also key for understanding plate driving forces. The realism of global circulation computations has advanced and such models with weak zones and other LVVs have led to an improved match to observed plate tectonic scores. Those include the correlation with plate motions, the magnitude of intra-plate deformation, and oceanic to continental plate velocity ratios. Net rotation of the lithosphere with respect to the lower mantle may be caused jointly by regional slab forcing and the stirring effect of cratonic keels. However, slab models have so far only produced net rotations that are small compared to recent hotspot reference-frame models. Progress in the next years will likely come from a better understanding of slab strength, which is still uncertain since large-scale subduction zone observables and laboratory results do not put strong con-

straints on slab rheology. Importantly, circulation models with an improved representation of convergent margins will help to close the gap between regional and global approaches to subduction, and to better understand the potential role of the overriding plate.

Keywords: Plate velocities – subduction – trench rollback – numerical geodynamics

1 Introduction

Models of Earth's mantle dynamics can be tested with the surface observables that are provided by plate tectonic motions. Such analysis can address questions including those about the nature of the plate driving forces, the magnitude of plate-mantle coupling, and the strength of the lithosphere and asthenospheric mantle. Several lines of evidence point toward the importance of the subduction process for all of these issues, implying that models of slab dynamics may provide important clues for understanding the workings of plate tectonics. Sinking of dense material in a Stokes fluid captures a range of subduction zone observations, but trench kinematics are complicated by significant dissipation in the bending oceanic lithosphere, moving trenches, and lateral viscosity variations (LVVs). While a comprehensive, theoretical description of such effects is, notably, still missing, this paper strives to summarize the state of knowledge and may so provide a basis for future analysis.

Models of subduction have so far concentrated on two, complementary aspects: The first approach is global and focused on reproducing first-order observations, including force-balanced plate motions, the geoid, and tomographically-mapped, deep slab anomalies. Long-range forces due to global mantle circulation can be accounted for, but numerical modeling has not quite advanced enough to fully include regional plate-boundary dynamics at the required level of detail. It is therefore useful to pursue the second, "regional", approach to study how an isolated slab enters into the mantle and, by doing so, directly or indirectly exerts forces on the attached plates. Given the ease of analyzing the detailed processes inside a subduction zone, the regional approach is still most suitable for analysis of a specific geological setting.

Here, we wish to provide an overview of what has been learned about subduction dynamics from both approaches. We start with a review of observations of surface velocities and the implications of their vectorial character and spatial gradients (sec. 2). If relative motions and regional plate boundary and slab geometries are considered in isolation, Earth may be considered as provid-

ing “natural laboratories”. The degree to which individual subduction zones represent different realizations of the same general subduction experiment for different parameter values such as plate age is, however, debatable. It is not always clear if global or regional dynamics leads to local deviations from general trends.

Section 3 reviews results from global models for the role of slabs in driving plate motions. Important issues are the role of LVVs, such as due to continental roots, for affecting relative plate speeds and absolute reference frames; both are relevant if regional plate boundary dynamics are to be inferred from kinematic parameters. Subsequently, we discuss regional modeling (sec. 4), including some of the current technical limitations, and then tie those results back into the global plate tectonic picture.

Given the subject matter, we have to be subjective in the choice of material but refer the reader to subduction reviews on different aspects of the problem in the text. “Lithosphere” will be used synonymously with “plate” for simplicity, and contrasted to the weaker “mantle” including the asthenosphere; abbreviations and symbols used are given in Tables 1 and 2. We wish to distinguish between relatively high and low viscosity (and density) fluids, glossing over complications such as thermo-chemical effects. Those are often neglected in the experiments, either by necessity in the lab, or for simplicity in the numerics. The hope is that more realistic systems will obey the same rules as long as their averaged properties match the continuum, effective behavior. We refer to both numerical computations and laboratory analog work as “experiments”, as they ideally follow the same, basic laws of physics (*i.e.* conservation of mass, momentum, and energy), and both can be used to discover new (“emergent”) phenomena, or higher-level rules on system behavior.

2 Kinematic constraints from plate tectonics

From a dynamical point of view, the motions of the lithospheric plates are part of the mantle convection system, namely that of the upper boundary layer. However, this boundary layer is not only cold, but also stiff, and weakened at the plate boundaries. Plate tectonics is therefore unlike iso-chemical and isoviscous convection (*e.g.* Bercovici et al., 2000; Tackley, 2000a). A simplified view of plates as a thermal boundary layer is probably closest to the truth within the oceanic plates. Plates with large continental areas behave differently, partly because of their thicker, positively buoyant crustal packages and partly because of the underlying tectosphere (Jordan,

1978). There, volatile depletion due to melting in the past may be even more important in increasing plate strength than within oceanic plates (*e.g.* Lee et al., 2005).

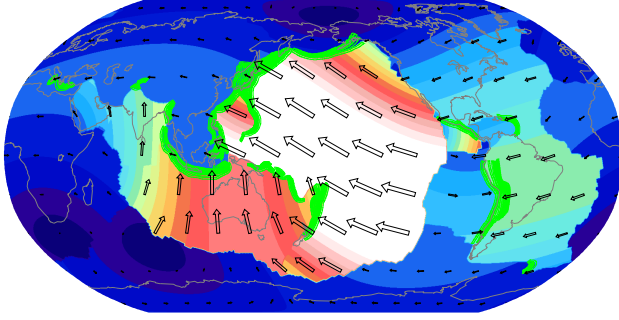
The long-term cooling of the Earth is mainly through the oceanic plate system, which is in turn dominated by the subduction process. However, oceanic plate convection is likely co-determined by continental formation and motion cycles (*e.g.* Lenardic et al., 2005; Zhong et al., 2007). An example of such interactions highlighted below are the lateral viscosity variations between stiff keels and weak sub-oceanic asthenosphere. Those affect relative plate speeds, observations of which have been used to infer slab force transmission. Moreover, LVVs due to keels also induce net rotations of the lithosphere with respect to the lower mantle. Such global, absolute reference frame motions are, in turn, important when regional subduction kinematics are to be extracted.

2.1 Global plate motions

Figure 1 shows two endmember representations of global crustal velocities at present. Model HS-3 by Gripp and Gordon (2002) (Figure 1a) is an example of a rigid, plate-tectonics model in the sense of McKenzie and Parker (1967) and Morgan (1968). The surface is subdivided into 15 major plates with relatively well constrained Euler vectors. When velocities are plotted as in Figure 1, it is apparent that the plates that have slabs attached to them move faster than those without. Moreover, the correlation between speed and length of attached trench, relative to plate circumference, is stronger than the inverse relationship with continental area (Forsyth and Uyeda, 1975). This is still one of the strongest indications for the importance of subduction for driving plates.

Relative motions in HS-3 are representative of the last 5.8 Ma and are from NUVEL-1A (DeMets et al., 1994). When continental regions with active deformation are excluded, satellite geodetic measurements, available for the last ~ 25 years, typically yield similar Euler vectors (*e.g.* Sella et al., 2002). However, any such geologic and geodetic data can only constrain relative motions, and further assumptions are required to define an absolute reference frame. For HS-3, it is of the hotspot kind, and was inferred from ten Pacific ocean island age progressions (Gripp and Gordon, 2002). The idea behind hotspot reference-frames is that oceanic islands may be caused by thermal plumes which rise from the deep mantle (Morgan, 1971; Wilson, 1973). In the most common approach, strictly stationary hotspots then define a reference frame with respect to the lower mantle (*e.g.* Minster and Jordan, 1978). Relative motions between hotspots are in

(a) HS-3, hotspot reference frame



(b) GSRM, no-net-rotation reference frame

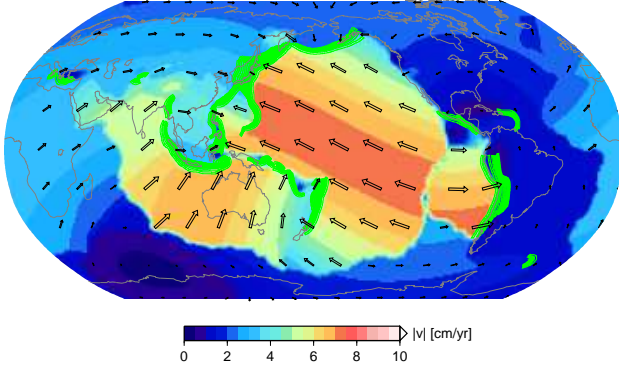


Figure 1: Crustal velocity amplitudes (background shading) and directions (vectors). (a) From the rigid-plate, hotspot reference frame model HS-3 by Gripp and Gordon (2002) (expanded on a $0.25^\circ \times 0.25^\circ$ grid). (b) From the deforming, no-net-rotation reference frame model GSRM by Kreemer et al. (2003) (on a $1^\circ \times 1^\circ$ grid). Green contour lines indicate slab seismicity from Gudmundsson and Sambridge (1998) (See online publication for color versions of Figures.)

fact \sim one order of magnitude smaller than plate motions (Molnar and Stock, 1987; Tarduno et al., 2003). Such motions are quantitatively consistent with plumes if the lower mantle convects more sluggishly than the upper mantle because of its higher viscosity (Steinberger et al., 2004; Boschi et al., 2007).

Spatio-temporal deviations from the assumption of constant motion of rigid plates, *i.e.* intraplate deformation (*e.g.* Gordon, 2000), can be most easily constrained with satellite geodetic measurements. If one chooses to represent the velocities by subdivision of the large plates into micro-plates, this often yields a regionally sufficient description (*e.g.* McClusky et al., 2000), but many micro-plate Euler vectors are still not well constrained (Bird, 2003). Figure 1b displays an example of an alternative approach, the GSRM model by Kreemer et al. (2003). Intra-plate deformation is allowed in certain, data-rich re-

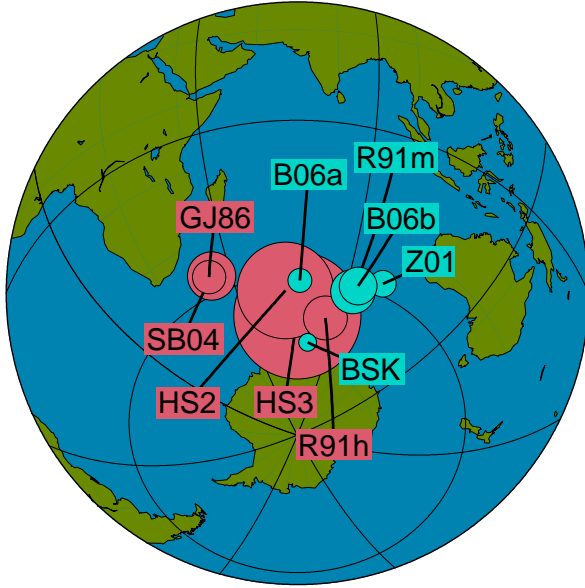
Table 1: Symbols used

| parameter | symbol |
|---|--|
| slab dip angle | δ |
| radius of Stokes' sphere | a |
| bending radius | R |
| slab/plate width | W |
| along-slab length in mantle | L |
| plate extent at surface | l |
| convective scale (mantle thickness) | H |
| area factor | $A = \frac{2\sqrt{HW} + \sqrt{Wl}}{H}$ |
| velocity vector | \vec{v} |
| trench normal velocities defined in Figure 3 | $V_T, V_P, V_{OP},$ $V_C, V_B,$ and V_S |
| Stokes velocity | V_{Stokes} |
| modified Stokes (bending) velocity (eq. 7) | V' |
| slope of the V_T/V_P anti-correlation | α |
| Stokeslet slowing factor | s |
| gradient operator | $\vec{\nabla}$ |
| pressure | p |
| deviatoric stress tensor | $\boldsymbol{\tau}$ |
| gravitational acceleration | $g = \vec{g} $ |
| density | ρ |
| density anomaly | $\Delta\rho$ |
| viscosity | η |
| mantle viscosity | η_m |
| slab/Stokes sphere viscosity | η_s |
| slab/mantle viscosity ratio | $\eta' = \frac{\eta_s}{\eta_m}$ |
| lower/upper mantle viscosity ratio | $\eta_l = \frac{\eta_{lm}}{\eta_{um}}$ |
| effective visco-plastic viscosity | η^{eff} |
| spherical harmonic degree | ℓ |

gions (compare, *e.g.*, SE Asia in Figures 1a and b), and inferred from geodetic measurements and geologic fault offset rates. Treated as a medium with viscous, continuous deformation, the crustal strain-rates can then be used to infer lithospheric and mantle rheology (*e.g.* England and Molnar, 1997).

2.2 Poloidal and toroidal velocities and reference frames

It is instructive to decompose velocity fields into poloidal, \vec{v}_p , and toroidal, \vec{v}_t , components. Poloidal flow corresponds to pure sources and sinks in the horizontal plane ($\vec{\nabla} \times \vec{v}_p = 0$), and is associated with vertical mass transport. Toroidal motion corresponds to vortex-like flow



| model | lon [°E] | lat [°N] | rate [°/Ma] |
|-------|-------------|-------------|----------------|
| HS3 | 70 | -56 | 0.44 |
| HS2 | 65 | -49 | 0.33 |
| SB04 | 38 | -40 | 0.17 |
| GJ86 | 37 | -40 | 0.12 |
| R91h | 84 | -56 | 0.15 |
| R91m | 93 | -47 | 0.15 |
| Z01 | 103 | -42 | 0.09 |
| B06a | 71 | -46 | 0.08 |
| B06b | 94 | -45 | 0.13 |
| BSK | 76 | -63 | 0.06 |

Figure 2: NR Euler poles, circle radius scales with magnitude. Red (light) symbols are from plate reconstructions with the stationary hotspot assumption (GJ: Gordon and Jurdy (1986), R91h: Ricard et al. (1991) using NUVEL, HS-2: Gripp and Gordon (1990), and HS-3: Gripp and Gordon (2002)), and allowing for flow-advected plume conduits (SB04: Steinberger et al. (2004) and pers. comm., B. Steinberger). The blue (dark) symbols are from the simplified continent/ocean shell model of Ricard et al. (1991) (R91m), and from full circulation models; Z01: global slab model with deep cratonic keels by Zhong (2001), B06a and B06b: using shallower keels, tomographic anomalies, and a temperature-dependent, power-law (a) and lab-derived, effective diffusion/dislocation creep rheology (b, η_{eff}), respectively (from Becker, 2006), and BSK: a computation that has no keels and whole mantle slabs (*cf.* Figure 6). For the B models, NR components were scaled such that the NNR velocities match NUVEL-1 RMS values (see Becker, 2006, for details and unscaled representation).

and rigid body rotations ($\nabla \cdot \vec{v}_t = 0$). The types of plate boundaries where poloidal and toroidal velocity amplitudes are largest are spreading centers and subduction zones, and transform faults, respectively (*cf.* O’Connell et al., 1991; Dumoulin et al., 1998; Tackley, 2000b). In a minimum viscous-dissipation configuration, Cartesian isoviscous convection will only contain poloidal flow. However, both spherical geometry and lateral viscosity variations will make a substantial toroidal flow component energetically favorable (O’Connell et al., 1991; Olson and Bercovici, 1991; Bercovici et al., 2000).

If plate velocities are expressed with spherical harmonics in terms of poloidal and toroidal fields, the degree one toroidal harmonic represents an average, rigid-body motion of the entire lithospheric shell (net rotation, NR, component). In Figure 1b, velocities from GSRM are in the no-net-rotation (NNR) reference-frame, defined by the requirement that the NR is zero. Hotspot reference-frames often show non-zero NR, and the relatively strong net-rotation component of HS-3 is apparent for Figures 1a and b. The NR corresponds to a mean velocity of 3.8 cm/yr, with maximum values reaching 4.9 cm/yr, enhances NW-

Table 2: Abbreviations used.

| abbreviation | meaning |
|--------------|--|
| APM | absolute plate motions |
| FE | finite elements |
| GSRM | global strain rate model of Kreemer et al. (2003), NNR surface velocities used here |
| HS-3 | hotspot reference frame velocities in the rigid-plate model of Gripp and Gordon (2002) |
| LVVs | lateral viscosity variations |
| NR | net rotation component of surface velocities |
| NNR | no net rotation reference-frame |
| TPR | toroidal to poloidal velocity field component RMS ratio for $\ell \geq 2$ |

ward velocities in the Pacific, and reduces the motion of Africa.

NR components for several hotspot reference-frames are shown in Figure 2. The sense of motion is similar for all models, but amplitudes depend on parameters such as the Euler poles for slow-moving plates (*e.g.* Africa) and, importantly, the geographic selection of hotspots (*e.g.* Ricard et al., 1991; O’Neill et al., 2005). HS-3 shows the strongest NR of the models in Figure 2, and we consider it as an endmember case that, by focusing on the Pacific hotspots, might overestimate NR motion. Model SB04 (Steinberger et al., 2004) allows for motions of hotspots with respect to each other; this reduces the amount of net rotation compared to HS-3. The NR is then slightly larger for SB04 than for GJ86 (Gordon and Jurdy, 1986) and of the same order as R01h (Ricard et al., 1991).

The excitation mechanism(s) for net rotations are still not universally agreed upon (*e.g.* Dogliani et al., 2007), but LVVs are a necessary condition (Ricard et al., 1991; O’Connell et al., 1991). The most likely explanation is that a combination of weak zone geometry (Bercovici, 2003) and strength contrasts between sub-continental and sub-oceanic asthenosphere (Ricard et al., 1991; Ribe, 1992) contributes to NR. Global convection computations by Zhong (2001) and Becker (2006) show that the right sense of motions is predicted (blue symbols in Figure 2) if LVVs and stiff cratonic keels are accounted for. We will return to net rotation excitation in sec. 3.5.

From a kinematic point of view, it is apparent that several plate motion characteristics are affected by the reference frame. The overall toroidal-poloidal partitioning is a trivial case with the $\ell = 1$ NR component (O’Connell et al., 1991). For $\ell \geq 2$, the ratio between global toroidal and poloidal RMS power (TPR; *e.g.* Tackley, 2000b) is ≈ 0.53 for all NUVEL-type models such as HS-3 and ≈ 0.57 for GSRM as in Figure 1. TPR has been at comparable levels (between 0.49 and 0.64) since 120 Ma (Lithgow-Bertelloni et al., 1993). Further, the ratio of the mean velocities within oceanic or continental regions depends somewhat on the net rotation component. For HS-2 (Gripp and Gordon, 1990), HS-3 and GSRM-NNR, for example, the values are ~ 2.55 , 2.05, and 1.55, respectively. This ratio, or that of the plates with predominantly oceanic or continental area, is of interest, as it has been used to infer the strength of slab pull and plate driving forces (Forsyth and Uyeda, 1975; Conrad and Lithgow-Bertelloni, 2002; Becker, 2006).

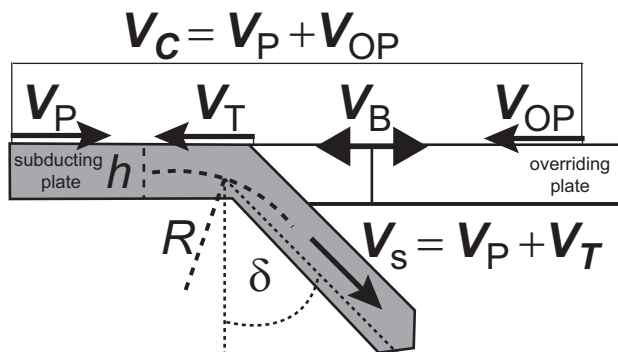


Figure 3: Regional subduction zone kinematics and slab geometry parameters. We assume that all intra-plate deformation is localized in the back-arc deformation rate, V_B (positive for extension), and all velocities are trench-normal components. Plate (V_P), trench (V_T , positive for rollback) and overriding plate (V_{OP} , positive toward the trench) velocities are all computed in an absolute reference frame. The convergence rate at the trench, V_C , is given by $V_P + V_{OP}$ with this sign convention, and the sinking velocity of the slab, V_S , is partitioned between V_P and V_T . (We assume $V_T = V_{OP} + V_B$, so $V_S = V_P + V_{OP} + V_B$.) We also indicate the width of the slab and plate, h , and the approximate bending radius at the trench, R , as well as the slab dip angle, δ . For more elaborate dip angle descriptions, see Jarrard (1986) and Lallemand et al. (2005).

2.3 Regional subduction kinematics and trench migration

Modeling subduction requires a choice of absolute reference frame because a layered mantle may produce slab anchoring at depth. Typically, absolute plate velocities relative to a hypothetical stagnant lower mantle are considered, for which hotspot reference-frames may be used. The kinematic parameters necessary to describe subduction also need to take into account the motion of the fore-arc sliver, which yields information on the kinematics of the trench. There is a long tradition of analyzing the dependence of the various kinematic (*e.g.* V_P) and geometrical (*e.g.* δ) quantities for different subduction zones to test how those are affected by parameters such as slab pull, parametrized by subducting plate age (see Figure 3 for the definitions).

A recent review of the role of the overriding plate, the subducting plate, and mantle flow in controlling subduction is given by Heuret and Lallemand (2005). It is now clear that strong correlations between dynamic and kinematic, or geometrical, quantities only exist for a few cases (*e.g.* Carlson and Melia, 1984; Jarrard, 1986; Cruciani et al., 2005; Heuret and Lallemand, 2005; Lallemand et al., 2005; Sdrolias and Müller, 2006). An extreme

view is to take such complications as sufficient evidence to abandon slab pull as a plate driving force (Doglioni et al., 2007). Alternatively, we think that the complications in deriving simple rules for slab behavior indicate that real subduction zones are more complicated than simplified considerations (*e.g.* McKenzie, 1969; Stevenson and Turner, 1972; Forsyth and Uyeda, 1975), and assumptions about steady-state subduction rates, would lead us to expect. As we show below, more realistic models of subduction provide physical explanations for many of the general trends.

Trenches are not stationary features, but are often found to retreat toward the subducting plate with respect to the lower mantle ($V_T > 0$; Spence, 1977; Chase, 1978; Garfunkel et al., 1986). However, it has been recognized that in several regions, *e.g.* Marianas-Izu Bonin, trenches also appear to advance toward the subducting plates in all reference frames ($V_T < 0$; Carlson and Melia, 1984; Jarrard, 1986; Heuret and Lallemand, 2005; Faccenna et al., 2007). Any trench migration has important consequences for tectonics such as back-arc spreading, but also for large-scale upper mantle dynamics. Modifications in the oceanic plate areas and trench locations will affect long-term heat transport and mixing efficiency of mantle convection. Regionally, the motion of trenches is also of importance since the details of mantle flow will be affected. The migration of the slab inside the mantle induces a toroidal component of flow, with significant effects on back-arc temperatures, volcanism, and the interpretations of seismic anisotropy observations (sec. 4.4).

As illustrated in Figure 3, V_T can be estimated by subtracting the back-arc deformation rate, V_B , from the velocity of the upper plate, V_{OP} (Carlson and Melia, 1984; Heuret and Lallemand, 2005), assuming that erosion and accretion at trenches are negligible (Lallemand, 1995). Errors in V_T may then result if this assumption is not justified (Clift and Vannucchi, 2004), or from uncertain V_B which is only straightforward to determine for spreading oceanic seafloor (Sdrolias and Müller, 2006). The Andes are a classical example where shortening rates vary dramatically as a function of balancing technique (Kley, 1999). Given such geological complications, V_B can also be approximated by geodetic studies (Heuret and Lallemand, 2005; Doglioni et al., 2007) although the relevant time interval (compared to the seismic cycle) is not the same, and V_T might fluctuate over several Ma (Sdrolias and Müller, 2006; Schellart et al., 2007).

The most straightforward effect on trench motions, however, is that of the reference frame (Figure 4). Funicello et al. (2008) present an analysis of trench motions and find that almost all Pacific trenches are strongly af-

ected by the NR component, as expected from Figure 2. Generalizations on subduction zone behavior in terms of V_T trends should thus be treated with caution. A lower mantle reference-frame, presumably approximated by the hotspot models with significant NR components, is probably the most appropriate choice for subduction rollback studies, and the NNR reference-frame provides an end-member description for reduced NR.

Global V_T mean and standard deviation vary between 6 ± 40 mm/yr for HS-3 and 11 ± 30 mm/yr for NNR (Figure 4b, predominantly rollback). It is apparent, however, that the distributions are spread out, and the value of the mean might not be significant (note the bi-modality/skewness in Figure 4b). The geometric mean of the ratio of trench motion to subducting plate velocity is 0.48 for HS-3 and 0.3 for NNR (using data from Heuret and Lallemand, 2005), *i.e.* trench migration rates are typically not more than $\sim 50\%$ of the convergence rates.

3 Global mantle flow and subduction dynamics

What are the physical models of mantle convection that can explain the kinematic surface observations? Even if plates and subduction are simply aspects of the mantle system, there are still important lessons to be learned from subdividing the forces driving the plates into different components (“force models”, *e.g.* Solomon and Sleep, 1974; Forsyth and Uyeda, 1975; Chapple and Tullis, 1977); a short review may be found in Becker and O’Connell (2001).

Another approach is bottom up (“velocity model”) where one solves for mantle flow given specified density distributions and mantle rheology, and then evaluates the tractions that apply at the base of the plates. Density anomalies may be inferred for slabs from seismicity (Hager, 1984), subduction histories (Ricard et al., 1993; Lithgow-Bertelloni and Richards, 1995; Steinberger, 2000), or seismic tomography (Hager and Clayton, 1989; Forte and Peltier, 1987). We start with a short introduction of mantle fluid dynamics before discussing global flow models and their implications for the role of slabs and subduction for plate tectonics.

3.1 Stokes flow and circulation models

Inertial forces are negligible for the mantle (infinite Prandtl number limit), and continuity of momentum simplifies to the Stokes equation. For an incompressible fluid,

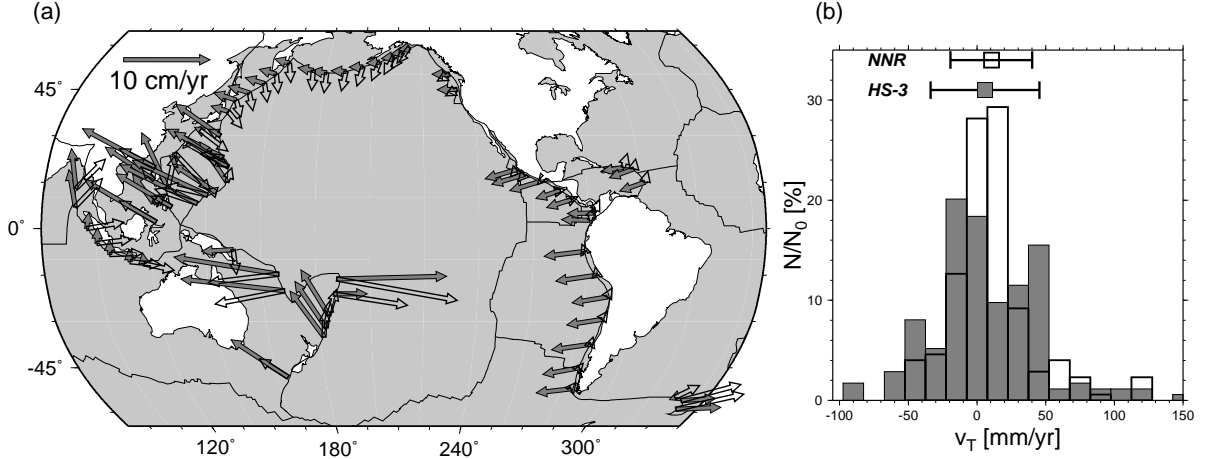


Figure 4: (a) Map of trench migration, V_T , for the present-day in the HS-3 (filled) and NNR (open vectors) reference frame (averaged on $7.5 \times 7.5^\circ$ blocks) and, (b), histograms of V_T . We show mean \pm one standard deviation on top of the histograms. Both figures are based on the even-length trench sampling by Heuret and Lallemand (2005) (cf. Funicello et al., 2008).

force balance can be written as

$$\vec{\nabla} p - \vec{\nabla} \cdot \boldsymbol{\tau} = \vec{g} \Delta \rho. \quad (1)$$

An important laminar flow problem with an analytical solution is that of a viscous sphere with η_s embedded in an infinite medium with viscosity η_m . For which the sinking, Stokes velocity is given by

$$V_{\text{Stokes}} = C \frac{\Delta \rho g a^2}{\eta_m} \quad (2)$$

with a viscosity-ratio dependent

$$C = \frac{2 + 2\eta'}{6 + 9\eta'} \quad \text{where} \quad \eta' = \frac{\eta_s}{\eta_m}. \quad (3)$$

For a rigid sphere ($\eta' \rightarrow \infty$), $C = 2/9$ and for a weak bubble ($\eta' \rightarrow 0$), $C = 1/3$, indicating that V_{Stokes} is mostly sensitive to η_m and not η' . Different orientations of an elongated sinker also do not affect C by more than a factor of ~ 2 (Batchelor, 1967). The $\eta_m/(\Delta \rho g a)$ term in V_{Stokes} sets a timescale for any buoyancy-dominated subduction problem, and scalings of $V \propto \Delta \rho a^2/\eta_m$, and $\tau \propto \Delta \rho a$ are expected. For typical values of $\Delta \rho = 50 \text{ kg/m}^3$, $a = 100 \text{ km}$, and $\eta_m = 10^{21} \text{ Pas}$ (e.g. Turcotte and Schubert, 2002), $V_{\text{Stokes}} \sim 4 \text{ cm/yr}$.

For a Newtonian fluid with constant η , eq. (1) further simplifies to

$$\vec{\nabla} p - \eta \nabla^2 \vec{v} = \vec{g} \Delta \rho. \quad (4)$$

where it can be seen that pressure gradients, $\vec{\nabla} p$, and viscous drag, $\eta \nabla^2 \vec{v}$ are balanced by the buoyancy forces, $\vec{g} \Delta \rho$. Without inertia, the mechanical boundary conditions

plus density distributions uniquely determine an instantaneous velocity solution ("circulation model"). Without LVVs, the Stokes flow problem is linear and this allows the superposition of solutions for the flow field of point-like buoyancy sources (e.g. Batchelor, 1967).

For super-critical Rayleigh numbers, subduction velocities can also be estimated from a fluid loop analysis of sinking plumes in an isoviscous convective cell (Turcotte and Oxburgh, 1967; Turcotte and Schubert, 2002). Energetically, any convective system will maintain a balance between the rates of potential energy change and the viscous dissipation (stress times strain-rates) in the fluid. How the latter partitions between the mantle and the plate may affect plate velocities (sec. 4.3.3).

3.1.1 Numerical solution methods

If surface velocities and internal density anomalies are prescribed, velocities and tractions can be computed easily in spherical geometry if mantle viscosity is assumed to be only radially variable (e.g. Hager and O'Connell, 1981; Forte and Peltier, 1987; Hager and Clayton, 1989). Such semi-analytical models can be solved in seconds on a modern computer, and their spatial resolution is limited mostly by the input density model, at present well resolved up to $l \sim 20$ for global seismic tomography (Becker and Boschi, 2002).

Earlier attempts to evaluate the role of LVVs in mantle flow were affected by modeling limitations (Čadek et al., 1993; Zhang and Christensen, 1993; Wen and Anderson, 1997). Iterative schemes such as that of Zhang and Christensen (1993) are usually restricted to small (\lesssim three or-

ders of magnitude) LVV, and the resolution of early direct solution methods was limited by available computer memory (Forte and Peltier, 1994). However, the ongoing increase in computational resources has brought partial remedy. Parallelization and improved algorithms have allowed computations of more realistic global models with spectral (Moucha et al., 2007) and finite volume or element (FE) methods (*e.g.* Tackley et al., 1994; Zhong et al., 2000). FE methods such as CitcomS (Moresi and Solomatov, 1995; Zhong et al., 2000) are well benchmarked and now jointly developed through CIG (geodynamics.org).

Spatial resolution of global models is now routinely at the ~ 25 km element size level and using CitcomS, for example, initial velocity solutions can be obtained within minutes to hours depending on the resolution, numbers of CPUs, the magnitude of LVV, and the solution algorithms used. However, strong LVV, such as for thin weak zones, can cause slow convergence of iterative solutions for \vec{v} . In such cases, care has to be taken to avoid intermediate and erroneous, but not obviously wrong-looking, solutions. Such issues should be solvable using improved multi-grid schemes and variable mesh refinement in the future.

3.2 Role of slabs for plate motions

An important advance in our modeling capabilities to test the consistency of tractions from circulation models with observed plate velocities was provided by Ricard and Vigny (1989). In their formulation, plates are assumed rigid, thin shells with no applied forces along their boundaries whose geometry is prescribed. One may then first compute the interaction of unit motions of one plate via viscous drag on another (Gable et al., 1991), and then solve for “free” plate motions so that the torques due to the body force loading are balanced.

Several workers have applied such velocity models to test force partitioning (Deparis et al., 1995; Lithgow-Bertelloni and Richards, 1995; Čížková et al., 1998), and plate motions can be fit well (linear correlation coefficients between observed and predicted Euler vectors ~ 0.9). Typically, $\sim 70\%$ of the driving forces are found to be caused by slabs, and the rest is mainly due to gravitational sliding (ridge push) (Lithgow-Bertelloni and Richards, 1998). Becker and O’Connell (2001) found that $\sim 40\%$ of the total slab contribution originates in the lower mantle for typical viscosity profiles such as those from Hager and Clayton (1989).

Traction scale with the density anomalies, which may be affected by both chemical and thermal effects (*e.g.* Forte and Mitrovica, 2001) and depend on inversion

choices when inferred from tomography. Another issue with velocity models is that the magnitude of force transmission from mantle flow to the lithospheric layer (“plate coupling”) depends somewhat on the radial viscosity structure. A moderate reduction in sub-lithospheric viscosity in the transition zone ($\eta \sim 10^{19} \dots 10^{20}$ Pas for depths $100 < z \leq 410$ km compared to $\sim 10^{21}$ Pas for $410 < z \leq 660$ km) is indeed preferred by inversions of geopotential and post-glacial rebound data (Hager and Clayton, 1989; Mitrovica and Forte, 2004), and also expected given laboratory constraints on upper mantle rheology (Hirth and Kohlstedt, 2004). However, Lithgow-Bertelloni and Richards (1998) and Becker and O’Connell (2001) showed that even for low transition zone viscosities of order $10^{18} \dots 10^{19}$ Pas, a large fraction of the forces driving the plates originates in the mantle. Put differently, a mantle contribution is required and lithospheric, gravitational potential energy variations alone cannot drive the plates. Becker et al. (2003) further explored the role of an asthenospheric low viscosity channel and found that seismic anisotropy prefers relatively strong coupling with global asthenospheric viscosities being no less than $\sim 10^{-3}$ of the upper mantle reference viscosity.

3.3 Edge forces *vs.* mantle drag

Can we use velocity models to make refined assessments for plate-boundary dynamics? Becker and O’Connell (2001) combined the force model approach of prescribing shear and normal forces along the plate boundaries with the velocity model of computing mantle tractions. These authors explored various combinations of forces and showed that velocity correlations were not very sensitive to edge forces. In the absence of LVV, adding asymmetric pull by slabs on plates did not improve the model fit much over models where tractions due to sinking slabs apply symmetrically at both overriding and subducting plate (“slab suction” in the terminology of Conrad and Lithgow-Bertelloni, 2002).

Figure 5 shows the reason for this force ambiguity: several of the plate driving and resisting forces are highly (anti-)correlated (Forsyth and Uyeda, 1975). This is because of plate geometry and motions from spreading centers to subduction zones: any edge-force derived torque that is based on plate boundary segments which are roughly perpendicular to plate motion will then yield similar forcing vectors. An exception is a plate-motion drag that applies underneath cratonic roots only (“plate motions at cratons” in Figure 5).

Conrad and Lithgow-Bertelloni (2002) presented a similar, joint force analysis and focused on the partitioning

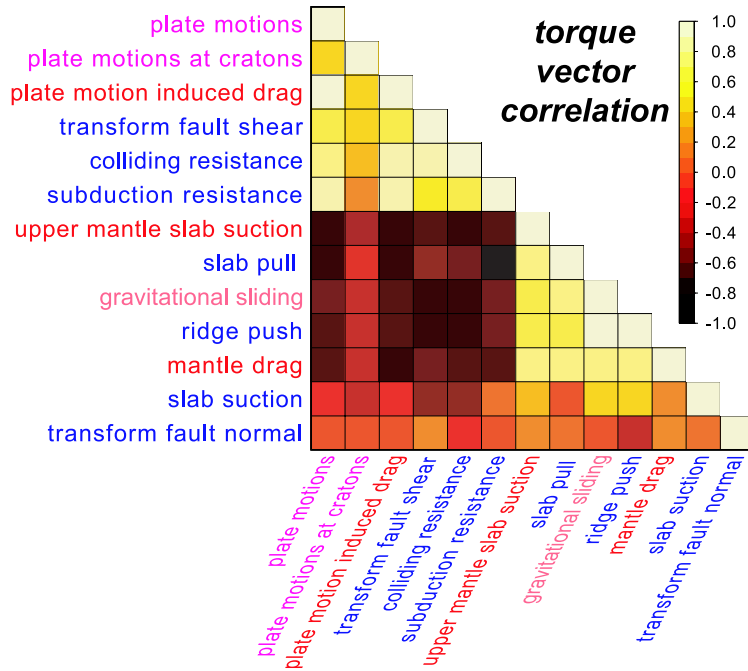


Figure 5: Correlation of torque vectors for all major lithospheric plates and several driving and resisting forces, modified from Becker and O’Connell (2001). We show edge forces in blue (dark) following the classification of Forsyth and Uyeda (1975), and forces computed from global circulation models in red (light gray; “slab suction” refers to the slab-density induced downwelling tractions, “mantle drag” to a tomography-inferred model which includes upwellings). “Gravitational sliding” is a gravitational potential energy model for the lithosphere that includes the distributed half-space cooling force, as opposed to “ridge push” which just applies at the spreading centers (lighter gray). All plate velocities were computed in the NNR reference-frame, for details see Becker and O’Connell (2001).

between slab suction and slab pull. In contrast to Becker and O’Connell (2001), these authors found that incorporating slab pull did improve plate motions significantly. Conrad and Lithgow-Bertelloni inferred a yield stress of ~ 500 MPa via the slab’s stress-guide behavior, and expanded their analysis to past convective settings (Conrad and Lithgow-Bertelloni, 2004) and thrust interface coupling (Conrad et al., 2004). It is likely that different assumptions about the details of plate boundary geometry and the resulting force integration may be responsible for the diverging conclusions. More importantly, Conrad and Lithgow-Bertelloni (2002) chose to not only consider correlations of plate motions, but also the ratio between oceanic and continental plate velocities, which is indeed increased if one-sided slab pull is added to the oceanic plates.

3.4 Lateral viscosity variations and variable plate coupling

Lateral variations in the plate-mantle coupling may be important for such velocity ratios, particularly if one considers the relatively stiff cratonic keel regions compared with the hotter and compositionally distinct sub-oceanic asthenosphere at ~ 200 km depth (Ricard et al., 1991; Zhong, 2001; Čadek and Fleitout, 2003). We can infer plate motions for LVV models by prescribing weak zones along plate boundaries (Zhong and Davies, 1999). Such computations are conceptually similar to the approach of Ricard and Vigny (1989), and have some limitations (*e.g.* effect of weak zone viscosity on plate speeds). Those are, however, fairly well understood (King and Hager, 1990; King et al., 1992; Han and Gurnis, 1999; Yoshida et al., 2001).

Following the work by Zhong and Davies (1999) several recent computations have advanced our understanding of global plate dynamics. Conrad and Lithgow-

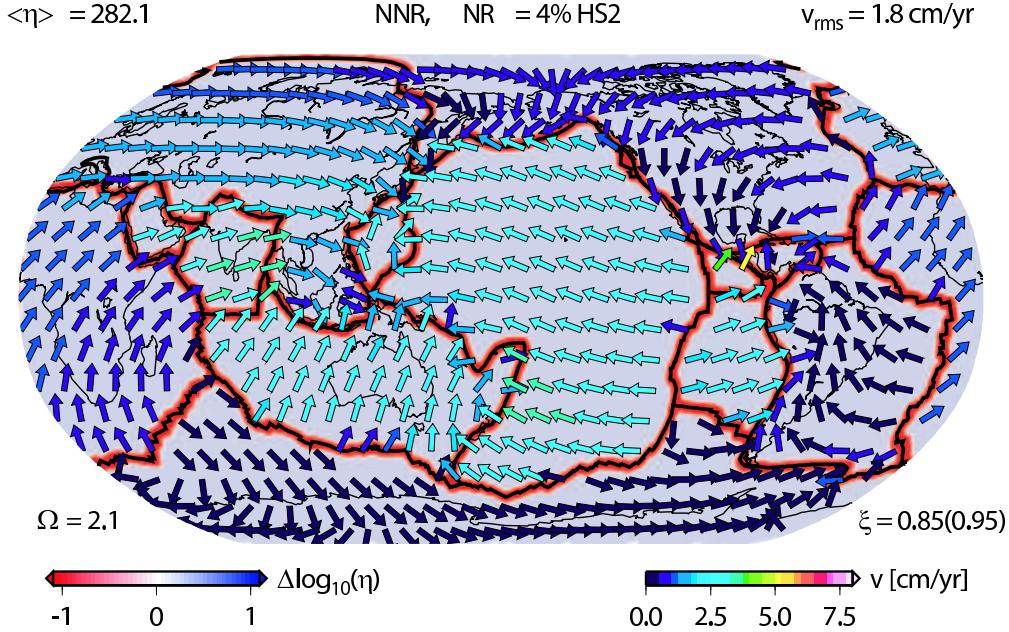


Figure 6: Surface velocities in the NNR reference-frame as predicted by an example computation following Zhong (2001). The rheology and model setup is similar to the η_{eff} model of Becker (2006) (B06b in Figure 2) but does not consider stiff cratonic keels, and only density anomalies from the slab model of Steinberger (2000) are used to drive flow. We show plate motions as vectors (fixed length, shading indicating amplitude) and lithospheric viscosity (weak zone geometry prescribed, mean viscosity, $\langle \eta \rangle$, is ~ 280 times the reference, 10^{21} Pas). The flow computation predicts only a small amount of NR flow ($\sim 10\%$ of HS-3 when corrected for RMS velocities, BSK in Figure 2). Velocities correlate with NUVEL-1 at the $\xi = 0.85$ (0.95 velocity weighted) level. The RMS ratio between oceanic and continental plates ($\Omega = 2.1$) is very similar to observations, while the overall RMS velocities (1.8 cm/yr) are too low; this could be adjusted by tuning the weak zone formulation or the density model.

Bertelloni (2006) evaluated the role of 3-D LVVs including continental roots on coupling and found that traction amplitudes are strongly affected by LVVs whereas directions are not. Becker (2006) computed global flow using a “realistic” rheology as expected for joint diffusion/dislocation creep for dry olivine in the upper mantle (Karato, 1998; Hirth and Kohlstedt, 2004). Becker found that mantle flow directions for models with LVVs were roughly similar to estimates with only radially varying rheology on global scales, but deviations exist regionally, especially underneath the oceanic plates. Importantly, the low viscosity asthenosphere underneath the oceans increases the plate velocities there, and so affects strongly the oceanic/continental velocity ratio (Figure 6).

Ricard and Vigny (1989)-type models with prescribed plate boundaries and plates that move freely as driven by density anomalies explain the observed plate motions well (Lithgow-Bertelloni and Richards, 1998). This means that computations where surface motions are prescribed at the surface and density anomalies drive additional flow (Hager and O’Connell, 1981) are dynamically consistent for adequate parameters. Such forward models can, of

course, not answer the question why the plate boundaries formed, but they can be used to explore how LVVs interact with plate tectonics. It is in fact possible to match several global plate tectonic scores (velocity ratios, correlations, plateness, TPR ratios) better with LVV models than with purely radially varying viscosity (Zhong, 2001; Becker, 2006). The lower viscosity asthenosphere facilitates oceanic plate motions and the temperature-dependent rheology reduces the intra-plate deformation such that it is similar to that found in GSRM as shown in Figure 1b (*cf.* Moresi and Solomatov, 1998). Even simple models such as those of Becker (2006), which were not optimized to fit plate motions, are able to match both directions (weighted correlations of ~ 0.9), and amplitudes of relative plate motions in continental and oceanic regions, without the addition of edge forces (Figure 6).

These conflicting findings as to the role of slabs for plate driving forces imply that global plate motions may be only moderately sensitive to the variation in plate boundary strength, though this clearly needs to be explored further with models of higher regional realism (*cf.* Billen and Gurnis, 2003). Other global datasets such

as the crustal stress field show similar non-uniqueness with regard to the role of deep slabs (Steinberger et al., 2001; Lithgow-Bertelloni and Guynn, 2004), while regional models provide a clearer detection of slab-induced flow for seismic anisotropy and stress (Becker et al., 2006; Humphreys and Coblenz, 2007).

3.5 Net rotations caused by keels and slabs

Another subduction-related prediction of LVV circulation models are net rotations which are relevant to determining regional kinematics (Figures 2 and 4). Toroidal flow can be excited by LVVs within the lithosphere (*e.g.* Tackley, 2000b,c), and $\ell = 1$ NR motion by continent–ocean asthenosphere viscosity differences (Ricard et al., 1991). The role of stiff keels was first studied with full flow solutions by Zhong (2001). The net rotations that are excited for power-law rheologies and large-scale tomographic anomalies as used by Becker (2006) are somewhat higher than those found by Zhong, even for shallower continental roots (Figure 2), and the sense of motion (pole location) is close to that of the hotspot reference-frames. However, the amplitude of the NR is always under-predicted for any of the published geodynamic models compared to HS-3.

Given the uncertainties in establishing hotspot reference frames, the NR component of HS-3 may be an overestimate. Moreover, geodynamic forward modeling of flow and azimuthal seismic anisotropy indicates that only a moderate amount of NR shear flow (as in GJ86 or SB04 of Figure 2) is consistent with seismology (Becker, 2008). However, accepting an under-prediction of NR from keel-based flow models for sake of argument, Becker (2006) suggested that it might be the joint effect of regional slab dynamics, buoyant upwellings, and continental keels that leads to higher NR motion than in the simplified flow models. Slab-induced NR flow was studied first on a global scale by Zhong (2001), with relatively low resolution computations. Slab interaction with the viscosity contrast at 660 km as a source for NR was discussed by Enns et al. (2005) for regional, two-dimensional (2-D) models, and is also implicit in the success of the Faccenna et al. (2007) predictions we discuss in sec. 4.4.2. We thus conducted further tests of this suggestion by computing LVV power-law flow for models that include slab structures.

Figure 6 shows velocities from an example circulation model that is based on converting the advected slablet model of Steinberger (2000) to temperature anomalies (*cf.* Zhong and Davies, 1999). We use the η_{eff} power-law rheology as in Becker (2006) (B06b in Figure 2), but did not prescribe any continental keels. The NR

amplitudes generated by slabs alone are relatively small (BSK in Figure 2), but the Euler pole location of HS-3 is matched well. (All NR amplitudes were normalized by the predicted NNR velocity RMS because other parameters were not optimized for these tests.) The induced NR roughly doubles if the additional effect of continental keels is considered, and different whole mantle slab models (Lithgow-Bertelloni and Richards, 1998) lead to similar results, confirming Zhong’s (2001) conclusions. We also conducted preliminary tests where we replaced upper mantle tomography by slab anomalies as inferred from seismicity (*cf.* Becker and O’Connell, 2001). For such upper mantle slab models, the role of keels was reversed, *i.e.* flow without keels yielded higher NR components than those which included keels. However, the NR component for any of these slab circulation models is $\lesssim 40\%$ of the original models by Becker (2006) (B06a and B06b in Figure 2) which include upwellings and downwellings as inferred from seismic tomography. These findings may imply that keel-deflected upwellings are more efficient than downwellings in NR excitation, but this needs to be confirmed with different slab and weak zone representations.

3.6 Flow confinement and geopotential fields

Lateral viscosity variations also need to be explored further in terms of the match of slab- and plate-induced flow to geopotential observations (Moresi and Gurnis, 1996; Chen and King, 1998; Zhong and Davies, 1999; Billen and Gurnis, 2001). Most global flow models without LVVs that employ a free-slip (zero shear stress) surface boundary condition (without weak zones along plate boundaries) match the geoid well, and plate motions poorly (because there is no toroidal flow). Alternatively, if plate motions are prescribed (“no slip” boundary condition with all velocity components fixed), these models lead to poor geoid fits (Thoraval and Richards, 1997). Studying slab-induced flow with LVVs, Zhong and Davies (1999) found that the fit to the geoid actually deteriorated when slabs were made stiffer than the mantle, and Čadek and Fleitout (2003) argued that impedance to flow at 660 km may be required by LVV flow models. Yet, Moucha et al. (2007) conclude that LVVs have a minor effect for geoid modeling based on tomography compared to uncertainties in the seismological models.

Such disagreement points to the requirement to incorporate diverse data into our geodynamical inversions, as velocity-related quantities are more sensitive to LVVs than stress-related measures, and the need to improve the

implementation of plate boundaries in spherical flow computations. Improved models would also allow better evaluation of suggestions of dynamic topography and pressure gradients (Phipps Morgan et al., 1995; Husson and Ricard, 2004) that may be induced by closing off parts of the mantle by “slab curtains”, such as around the Pacific at present. Husson et al. (2007), in particular, explored the influence of the Americas motion on the asymmetry of plate velocities in the Pacific. Such slab-imposed barriers to flow may also temporarily degrade thermal mixing with consequences for the coupling between oceanic plate convection and sub-continental heat budgets (*cf.* Lenardic et al., 2005).

The next few years will likely bring new insights into how a consistent description of geopotential, anisotropy, and plate motion data may be achieved with weak spreading centers and thermo-chemically strong, but plastically yielding, convergent margins in a global model. It is also desirable to understand regional dynamics fully before models are made more comprehensive. However, we start with a cautionary note for the interpretation of global quantities based on regional models.

3.7 Large-scale mantle wind and regional slab circulation

Figure 7 shows two numerically computed subduction zone “streamlines” (*cf.* Hager and O’Connell, 1978). Those examples are meant for illustration only and are not supposed to be particularly realistic. Figure 7a is for a regional box with a free-slip surface boundary condition; it shows typical, small-scale circular motion that is induced by the slab buoyancy and similar to a Stokes sinker. Moreover, it is evident that the box is not large enough to exclude the effect of the side boundaries. Importantly, the streamlines indicate that the slab dip that is input (inferred from seismicity) has substantially different alignment. Clearly, the reference frame of the overriding plate and trench motions needs to be considered for proper comparisons (*e.g.* Olbertz et al., 1997) but the mismatch between slab structure and flow in Figure 7a is typical even for more careful regional models.

If we prescribe plate motions on the surface in a global circulation model as in Figure 6, the regional circulation patterns are considerably simpler. Figure 7b shows a cut out of a global computation, but using an embedded, regional, high-resolution model yields similar results. Such nested models have recently been used in a unidirectional mode, where the large-scale flow determines the velocities on the sides of a smaller box (Mihálffy et al., 2007), and in a more sophisticated fashion where communication

goes both ways (Tan et al., 2006). (While the NR motions are not completely understood (sec. 3.5), such large-scale flow that is unique to LVVs should be accounted for in nested modeling approaches but has been neglected so far.)

For the example of Figure 7b, the subduction vortices are suppressed and the flow much simplified compared to Figure 7a. (This is not to say that actual mantle currents need to be simple; smaller-scale effects may be averaged out in global computations.) Moreover, the dip from seismicity matches with the flow lines, as was shown globally without LVVs by Hager et al. (1983). The computation of Figure 7b is not suited for quantitative comparisons strictly speaking, as a global subduction model with free surface conditions and weak zones should be used for consistency. However, since plate velocities of such models match the observed ones well, results would be very similar.

Subduction is likely a highly time-dependent process (*e.g.* Ita and King, 1998; Becker et al., 1999; Faccenna et al., 2001a; Billen and Hirth, 2007), and one may thus rightly argue that slab dips should not necessarily line up with instantaneous flow at all times (*cf.* Garfunkel et al., 1986; Lallemand et al., 2005). However, as earlier work on global flow and Figure 7 illustrate, it is important to at least evaluate the role of large-scale currents if insights from regional models are transferred to global observables such as slab dip. With this caveat, we turn to the modeling of isolated slabs.

4 Regional slab dynamics

Regional models of subduction, implemented mostly in 2-D, have been reviewed elsewhere with focus on deep dynamics and slab ponding at 660 km (King, 2001; Christensen, 2001), thermal structure (van Keken, 2003; King, 2007), and rheology (Billen, 2008). Recent advances include the incorporation of laboratory-derived rheologies to test how temperature-dependent viscosities plus plastic yielding may explain slab morphology (*e.g.* Čížková et al., 2002; Billen and Hirth, 2007), and what processes might assist subduction initiation (Toth and Gurnis, 1998; Faccenna et al., 1999; Regenauer-Lieb et al., 2001; Hall et al., 2003). However, as for the plate generation problem (Tackley, 2000a), questions remain about the appropriate weakening mechanism, the degree of strain history-dependence (*e.g.* Gurnis et al., 2000), and the effect of 3-D plate reorganizations and continental cover.

We proceed to comment on slab rheology, discuss some of the common assumptions inherent in regional, isolated slab models, and how assumptions are sometimes inter-

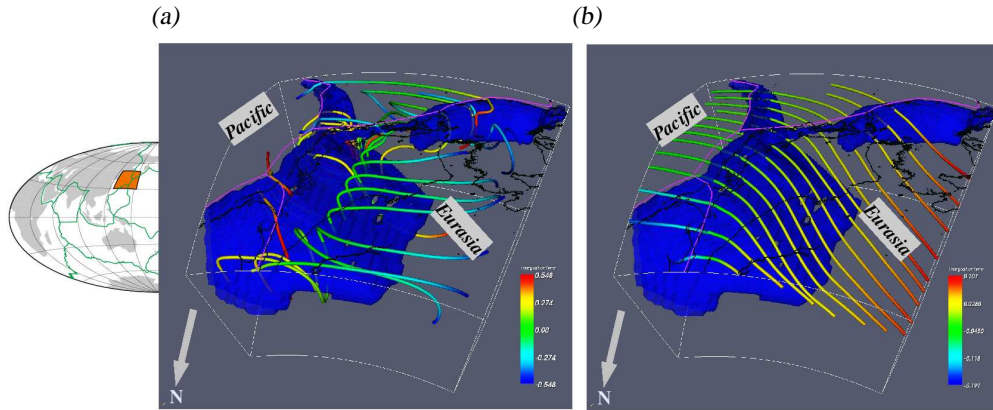


Figure 7: Illustration of the potential importance of large-scale flow for subduction zone observables. Circulation models include upper mantle slabs as inferred from seismicity (from Gudmundsson and Sambridge, 1998) within the Japan-Kurile system (blue/dark surfaces) which are converted to temperature anomalies, and are also stiffer than the mantle by a factor of $\eta' \sim 200$. Flow is visualized by assuming velocities are steady-state and following tracers forward and backward in time (coloring is integration time). Part (a) is from a regional computation with free-slip boundary conditions. Part (b) is a cut out of a global computation that has the same regional density contribution as (a) but prescribed plate motions everywhere on the surface.

twined with numerical issues by necessity. We will focus on fluid subduction models that are concerned with exploring the question of what actually controls the plate and plate boundary motions. In particular, we discuss those models that allow the trench to move self-consistently (“free trench”) and strive to understand the causes rather than the effects of trench motion.

4.1 Free and prescribed trench motions

It was seismic tomography that renewed interest in the role of trench migration in modifying the shape of subducting slabs, and several workers showed how variable motion of the trench can explain the observed “ponding” of fluid-like slabs at the 660 km phase transition (Griffiths et al., 1995; Gouillou-Frotier et al., 1995; Christensen, 1996). There, a negative Clapeyron slope of the olivine-perovskite/magnesiowüstite transition may be expected to inhibit subduction temporarily (Christensen and Yuen, 1984; Kincaid and Olson, 1987), though the likely viscosity increase between upper and lower mantle alone will also lead to changes in slab dip, flattening, or folding (*e.g.* Gurnis and Hager, 1988; Zhong and Gurnis, 1995; Enns et al., 2005). Weaker slabs and large rollback will promote ponding, whereas stationary, strong slabs are more likely to penetrate into the lower mantle (Davies, 1995; Christensen, 1996).

The migration of the slab inside the mantle also has an important impact on return mantle circulation and the way the resisting forces are partitioned between slab and mantle (Garfunkel et al., 1986; Conrad and Hager, 1999a). On

that premise, several recent studies consider the trench motion as a proxy to infer subduction dynamics (Bellahsen et al., 2005; Enns et al., 2005; Royden and Husson, 2006), rather than prescribing V_T . Such free trench models, where V_T evolves dynamically, were pioneered in laboratory analog modeling by Jacoby and Schmeling (1981). Kincaid and Olson (1987) focused on an isolated subducting slab and showed that rates of subduction and rollback could be strongly affected by the interaction of the slab with a viscosity or density contrast at depth. Shemenda (1994) presented a wide range of laboratory experiments for an elasto-plastic slab in an inviscid (water) mantle, with particular focus on lithospheric deformation and back-arc spreading. Zhong and Gurnis (1995) discussed 2-D cylindrical numerical experiments that included a mobile, faulted margin implemented using FE with slippery-nodes (Melosh and Williams, 1989). The numerical results confirmed that plate kinematics may depend strongly on deep slab dynamics. Faccenna et al. (1996) introduced a different kind of laboratory analog model to the subduction research community. Silicone putty and glucose syrup (both viscous at the strain-rates considered) fill the role of the lithosphere and mantle, respectively.

4.2 Impact of modeling assumptions

Rocks deform elasto-visco-plastically, depending on the timescales of loading and ambient conditions, and both numerical and laboratory subduction experiments have been performed with elasto-plastic, visco-elasto-plastic,

visco-plastic, and purely viscous rheologies. We will here focus on the latter two, but why would we expect that viscous slabs provide a sufficient description?

4.2.1 Rheology and viscous slabs

The role of elasticity in controlling slab-related deformation is in fact still somewhat controversial. Several large-scale features of subduction zones can be explained by elasto- or visco-plastic behavior, including the forebulge (Melosh and Raefsky, 1980; McAdoo et al., 1985; Zhong and Gurnis, 1994; Hall and Gurnis, 2005), the trench geometry (Morra et al., 2006; Schellart et al., 2007), and the shape of the slab (Hassani et al., 1997; Funicello et al., 2003b). These results indicate that macroscopic observations, *e.g.* trench geometry, alone cannot be used to infer slab rheology. Large-scale kinematics such as rollback trade-off with intrinsic parameters such as slab stiffness (*cf.* Billen and Hirth, 2007).

In terms of subduction dynamics, elasticity may play an important role in initiation of subduction (Kemp and Stevenson, 1996), forming instabilities or shear localization (Muhlhaus and Regenauer-Lieb, 2005; Kaus and Podladchikov, 2006), and might lead to enhanced slab rollback (Moresi et al., 2002). However, often different rheological laws are active in such models at the same time, and the specific role of elasticity is unclear. Kaus and Becker (2007) therefore evaluated an idealized problem, the development of Rayleigh-Taylor instabilities for viscous and visco-elastic rheologies. These authors found that the instability is sped up by the inclusion of elasticity, though only for parameter values that are likely not applicable to the Earth. For typical elasticity values as in PREM (Dziewoński and Anderson, 1981), stress fields are predicted to be different, but the temporal behavior of lithospheric instabilities is very similar for viscous and visco-elastic cases. While the effect of a supposed elastic core may need to be further explored, results by Schmeling et al. (2007) also indicate that elasticity does not significantly affect subduction dynamics.

Here, we shall therefore make the common assumption that the overall slab behavior over long time-scales can be well described by a visco-plastic fluid. Such an approach is supported by several lines of evidence: inferred intra-slab deformation from seismicity in Wadati-Benioff zones are on the same order of those expected for the fluid mantle (Bevis, 1986, 1988; Holt, 1995), the transition between in-slab extension and compression (Isacks and Molnar, 1971) can be explained by a fluid slab encountering a viscosity jump (Vassiliou and Hager, 1988; Tao and O’Connell, 1993), and both seismicity (*e.g.* Gardini and Woodhouse, 1984, 1986; Fischer and Jordan,

1991) and tomography (*e.g.* van der Hilst and Seno, 1993; Widiyantoro and van der Hilst, 1997) show strong slab contortions reminiscent of fluid behavior (*cf.* Christensen, 1996; Tan et al., 2002; Ribe et al., 2007).

4.2.2 Numerical models and analog experiments

To study fluid slabs, regional, 3-D numerical computations can now routinely be performed at relatively high resolution (*e.g.* Billen and Gurnis, 2003; Piromallo et al., 2006; Stegman et al., 2006). Figure 8 shows snapshots from typical visco-plastic, numerical models. Using CitcomCU (Zhong et al., 1998) with a standard resolution of ~ 20 km ($\sim 4,000,000$ elements) and ~ 80 advected material tracers per element, such computations take a few hours (using 54 CPUs) for a typical model evolving over tens of Myrs with thousands of time steps. However, the large LVVs that are inferred from laboratory creep laws still pose some problems numerically, particularly in the global, spherical case where thermo-chemical problems such as entrainment remain challenging. It is therefore very useful to also consider laboratory models.

Numerous tectonic processes may be studied with analog experiments, provided that adequate scaling of material parameters to nature is ensured (*e.g.* Weijermars and Schmeling, 1986). One of the motivations for modeling subduction with both analog and numerical models is to complement each method’s weaknesses and strengths. For the lab approach, pressure and temperature-dependence of rheology, reproducibility, and extraction of quantitative information are challenges, while physical realism and resolution can be strengths. The advantage of numerics is that all relevant quantitative measures can be easily extracted, and computer experiments can explore parameter space with perfect reproducibility.

The joint study of laboratory experiments and analytical or numerical methods has a long history in fluid dynamics (*e.g.* Ribe, 2003, for a related study). Applications to the subduction problem include the work of Kincaid and Olson (1987) who compared lab results on slab ponding with computer experiments by Christensen and Yuen (1984). Hassani et al. (1997) evaluated numerical models of elasto-plastic slabs following Shemenda (1994), and Becker et al. (1999) compared the analog models of Facenna et al. (1999) with numerics. In an effort to further reduce the complexities and to understand the role of the subducting lithosphere in isolation (Christensen, 1996), many subsequent analog experiments focused on a single (stiff, dense, fluid) plate and got rid of the overriding plate (*e.g.* Funicello et al., 2003a, 2004, 2006; Schellart, 2004a,b).

Assuming Moore’s (1965) law continues to hold, one

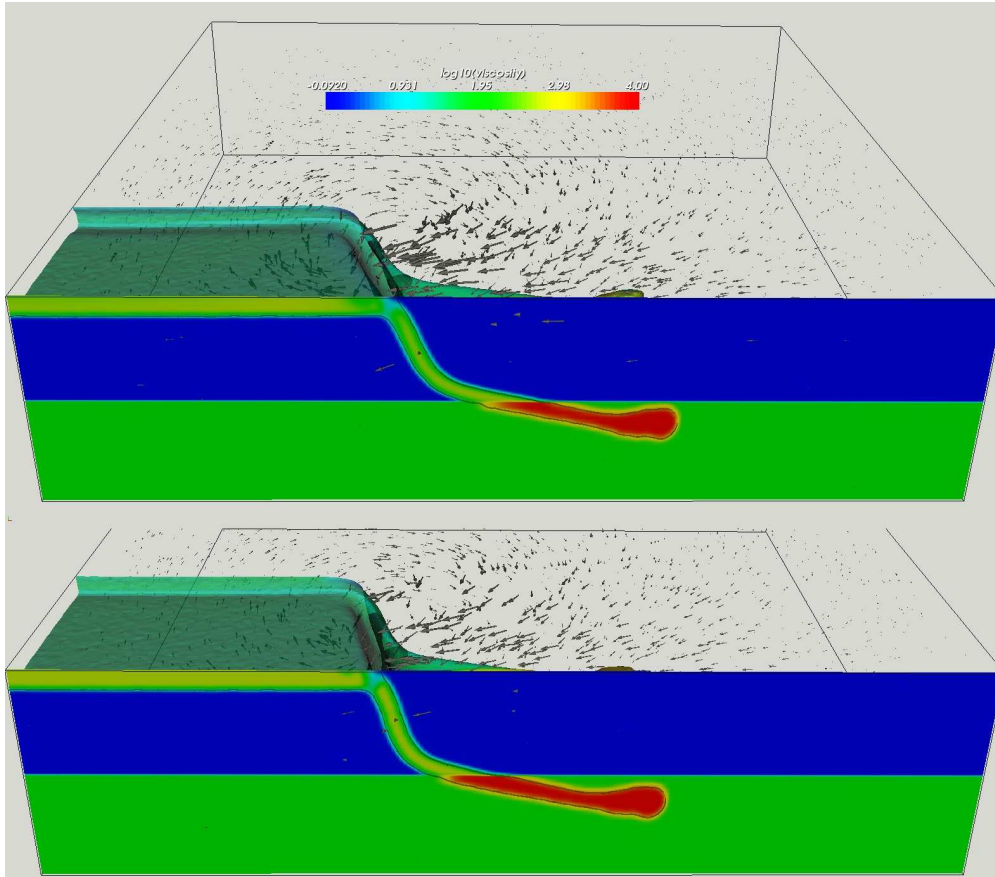


Figure 8: Example of regional, free trench computations focusing on understanding trench kinematics. A visco-plastic slab (green, compositional iso-surface) sinks into a mantle with viscosity stratification (see shading for \log_{10} of viscosity η^{eff}); black vectors denote flow velocity. Slab stiffness is $\eta' = 500$, lower/upper mantle viscosity ratio $\eta_l = 100$, and the subducting plate is attached to the side of the box on the left (“fixed ridge”, *cf.* Enns et al., 2005). Bottom figure is for the minimum implementation of viscoplasticity (eq. 6), top is for the same model setup and time step but using the average viscosity formulation, eq. (5). See Figure 10a for temporal evolution.

may expect that increased computing power may soon render analog experiments obsolete. However, the lab has been catching up with improved analysis techniques (*e.g.* particle velocimetry, temperature visualization via polymers). Besides methodological issues, there are also often implicit assumptions, *e.g.* with respect to boundary conditions, whose relevance may only become evident when different approaches are compared. This is further motivation to use different tools to tackle the same problem, and we next discuss an example of such issues which, ironically, stem from trying to reproduce the simplified, single-slab experiments.

4.2.3 The surface boundary condition and viscoplasticity

Most computations are conducted in an Eulerian framework with free-slip top surface boundary conditions. If an isolated, dense body is introduced on the top of the fluid domain, it is hard to detach the dense fluid from the top boundary in a slab-like shape, as opposed to a drip-like downwelling. This is because only horizontal motions are allowed at the top, and the corner flow geometry leads to a stress singularity in the wedge region (*cf.* Batchelor, 1967; Budiansky and Carrier, 1973). For kinematic subduction models, a similar wedge issue exists, and temperature solutions depend sensitively on discretization and choices on slab coupling (van Keken, 2003).

Several tricks are used to circumvent complications due

to the wedge, including the addition of a soft, buoyant surface layer. Artifacts due to soft layer entrainment may result, however, and different methods yield convergent solutions only under relatively high resolution (Schmeling et al., 2007). Schmeling et al. also show that the averaging method for the effective rheology close to material interfaces leads to extremely different results. Eulerian codes only match results from Lagrangian, free-surface numerics, or laboratory results, if the (weakest) harmonic averaging is chosen. Such averaging of two fluid viscosities corresponds to two dashpots in series, as would be appropriate for simple shear; for pure shear, the dashpots would act in parallel (arithmetic mean). Which averaging scheme applies to subduction in general is unclear (Schmeling et al., 2007).

Another way to detach the slab in free-slip computations is the use of “Byerlee (1978)” type plasticity to locally yield a strong slab (as in Figure 8). Taking this (pseudo-)plastic implementation as an example, Enns et al. (2005) argued that the introduction of a plastic viscosity, η_p , which is computed by dividing an appropriately adjusted, depth-dependent yield stress by the local strain-rates, allows detaching the slab without affecting its fluid behavior strongly. Such an approximate plastic behavior had been used before for subduction (Christensen, 1996; Tetzlaff and Schmeling, 2000), and is often also applied in plate generation studies (*e.g.* Moresi and Solomatov, 1998). This leads to another, secondary, issue: If one should treat plastic “viscosity” and the regular, creeping viscosity, η_c , as an effective viscosity (harmonic mean)

$$\eta_1^{\text{eff}} = \frac{\eta_p \eta_c}{\eta_p + \eta_c} \quad (5)$$

(*e.g.* Tetzlaff and Schmeling, 2000; Stein et al., 2004; Enns et al., 2005), or by using the minimum of the two viscosities

$$\eta_2^{\text{eff}} = \min(\eta_p, \eta_c) \quad (6)$$

(*e.g.* Moresi and Solomatov, 1998; Tackley, 2000b; Stegman et al., 2006). On the one hand, material should microscopically either behave plastically or viscously, which favors eq. (6). On the other hand, numerical resolution will typically be coarser than plastic shear zones, which favors eq. (5). Figure 8 shows two subduction models which only differ by the way this visco-plasticity is implemented. Differences are noticeable, but not large, for short time-histories, if sufficient resolution is used. However, subtleties such as different choices as to η^{eff} might partly explain, for example, why Stegman et al. (2006) were not able to closely reproduce Enns et al.’s (2005) results.

The extent to which viscous behavior dominates over plastic yielding in the models of Enns et al. (2005) is not

entirely clear, and we are testing truly viscous and visco-plastic slab behavior for free-slip and free-surface boundary conditions at present. These problems are emphasized by Stegman et al.’s (2006) visco-plastic models where the entire trench region of the subducting plate is weakened such that no in-slab forces are transmitted; bending dissipation is, consequentially, not important. Schellart et al.’s (2007) approach limits yielding to a crustal layer, which improves slab coherence.

In nature, a reduction of shallow lithospheric strength by brittle and ductile failure is expected from rock rheology (*e.g.* Brace and Kohlstedt, 1980; Burov and Diamant, 1995). Moreover, an increase in shallow weakening and faulting within the plate toward the trench is observed in plate flexure (McAdoo et al., 1985; Billen and Gurnis, 2005) and seismic (Ranero et al., 2003) studies, and deep slab deformation also requires departure from pure temperature-dependent viscosity (Čížková et al., 2002). However, we need to understand the rheological controls of the numerical and laboratory results better before confidently translating model results to nature. The importance of the trench formulation is also emphasized by the work of Royden and Husson (2006). These authors use a semi-analytical formulation to treat the effect of large-scale mantle flow and find that trench migration is less affected by deep dynamics, such as mantle flow, but more sensitive to the overriding plate density structure (*cf.* Shemenda, 1994).

4.3 Dynamic inferences from regional trench kinematics

Most of the previous caveats on methodology apply to inter-model comparisons. If parameters are varied within one fixed setup, useful insights on the overall dynamics can still be gained. We proceed to discuss explanations for the regional kinematics derived from fluid slab experiments and return to slab strength in sec. 4.3.3.

4.3.1 Back arc deformation and sinking velocities

Close to the trench, the overriding plate often deforms either in a strongly extensional sense (accommodated by back-arc spreading, “Marianas type”, $V_B > 0$) or in a compressional fashion (sometimes associated with orogeny, “Chilean type”, $V_B < 0$) (Uyeda and Kanamori, 1979). An overview of back-arc behavior and correlations of kinematic parameters with the style of deformation can be found in Lallemand et al. (2005).

Chase (1978) had argued that most slabs are either stationary or roll back in a hotspot reference-frame. The absolute overriding-plate motion would then control the type

of back-arc deformation, and we would expect a strong correlation between rollback (V_T) and back-arc extension (V_B). While multi-parametric descriptions can be found (Jarrard, 1986), real subduction zones appear to be more complicated (*e.g.* Carlson and Melia, 1984), and both trench motion and back-arc deformation are observed to vary in time (*e.g.* Sdrolias and Müller, 2006; Doglioni et al., 2007). Discrepancies between datasets built on geologic or geodetic observations may thus be expected. Newer data confirm the existence of correlation between V_B and overriding plate motion using back-arc deformation inferred from GPS geodesy (Heuret and Lallemand, 2005), although with large scatter. As for the causes of back-arc deformation, several processes are candidates. Large scale mantle currents that couple differently to slabs and via the thrust interface to the plate are among them (*e.g.* Dvorkin et al., 1993; Russo and Silver, 1994; Iaffaldano et al., 2006; Schellart et al., 2007), though it is unlikely that the diversity of deformation patterns can be explained by the effects of a single NR flow component as suggested by Doglioni (1990).

Heuret et al. (2007) provide a new analysis of global plate kinematics, back-arc deformation and deep slab shapes from tomography and seismicity (Heuret and Lallemand, 2005). In a plot of subducting (V_P) to overriding plate (V_{OP}) velocities, all of the Earth’s subduction zones fall along a negative trend that corresponds to overall convergence rates of roughly $V_C \sim 5$ cm/yr (with large $\sim \pm 50\%$ fluctuations). Back-arc spreading and steep dips are found toward large $V_P > 0$ and $V_{OP} < 0$, while shortening and shallow dips are observed for $V_P > 0$ and $V_{OP} > 0$.

Choices in the reference frame will affect the exact values of these kinematic parameters on Earth (Figure 4), *e.g.* if less NR than the HS-3 frame used in Heuret and Lallemand (2005) is applied. It is therefore more useful for broader conclusions to consider the overall slope of V_C . A general interpretation then emerges: if plates subduct with $V_C \gtrsim 5$ cm/yr, the overriding plate is shortened; it is extended for convergence rates $\lesssim 5$ cm/yr. It therefore appears that there is a preferred, local subduction rate V' which may be determined by regional slab dynamics and sinking into the mantle. If large-scale plate motions lead to values of V_{OP} and V_P that add up to deviations from V' , then back-arc deformation results. This “anchoring” effect of the slab is confirmed in laboratory experiments with piston-driven plates and stiff slabs ($\eta' \sim 1000$) where V_{OP} and V_P can be varied at will (Heuret et al., 2007).

If slabs were to consistently roll back, Heuret et al.’s (2007) observation would be in line with Chase’s (1978) original argument that the overriding plate motion con-

trols back-arc deformation. However, slabs are found to advance as well as retreat (Figure 4b), and such, more complex, behavior is expected for stiff slabs (Bellahsen et al., 2005). Sdrolias and Müller (2006) analyze the temporal evolution of back-arc spreading using O’Neill et al.’s (2005) hotspot reference-frame and age reconstructions. These authors find that back-arc extension is limited to old oceanic lithosphere, and always preceded by overriding plate retreat away from the trench. After extension is initiated, rollback and regional slab dynamics appear to play a role, consistent with the arguments by Heuret et al. (2007) based on laboratory experiments.

4.3.2 Stokes sinkers and tomography

If back-arc deformation is controlled by a sinking velocity V' , what controls this preferred subduction speed that would lead to deformation-neutral behavior? The first candidate for any velocity scale is $V_{\text{Stokes}} \propto \Delta\rho/\eta_m$ (eq. 2) and this is reflected in the findings of Capitanio et al. (2007) for density- or age-dependent slab velocities. However, disagreements arise over the origin and the degree of variations from such general Stokes-scaling. Processes such as thrust interface coupling at the margin, large-scale mantle flow, and lithospheric bending may additionally affect the actual subduction velocity (*e.g.* Conrad and Hager, 1999a; Becker et al., 1999; Buffett and Rowley, 2006), and deep slab interactions, such as at the 660 km phase transition will lead to further complications (*e.g.* Zhong and Gurnis, 1996; Faccenna et al., 2001b). However, assuming that mantle drag is the important control ($V' \approx V_{\text{Stokes}}$) and that slabs are weak, it is instructive to explore which other aspects of global subduction dynamics may be explained with Stokes behavior.

Seismic tomography images fast anomalies in the lower mantle which can be interpreted as continuous, cold slabs at least down to ~ 1200 km (*e.g.* Grand et al., 1997; Kárason and van der Hilst, 2000), and relative trench motion has a strong control on slab morphologies. Ricard et al. (1993) and Lithgow-Bertelloni and Richards (1998) therefore constructed a forward model of mantle structure by dropping “slablets” (superpositions of numerous Stokes sinkers) into the mantle at the locations where trenches are reconstructed to have been within the last 120 Ma. Lithgow-Bertelloni and Richards found that large-scale patterns in tomography can be matched well with such a model if the sinking velocity of the slablets is reduced in the lower mantle by a factor of $s \sim 4$. We expect $s \sim \ln(\eta_l)$, where η_l is the viscosity ratio between lower and upper mantle, because reduced sinking velocities (due to $\eta_l > 1$ and eq. 2) are accompanied by slab thickening in the lower mantle (Gurnis and Davies, 1986;

Richards, 1991). The best-fit slowing factor $s \sim 4$ is compatible with estimates of $\eta_l \sim 50$ from geoid modeling (e.g. Hager and Clayton, 1989).

The correlations between slablet model and tomography are mostly limited to the longest spatial wavelengths and only ~ 0.4 when computed up to $\ell = 8$, but the match holds up for comparisons with more recent tomographic maps (Becker and Boschi, 2002). Using the same subduction history as Ricard et al. (1993) but allowing for lateral advection of slablets by mantle flow as induced by changing plate motions and density anomalies (Steinberger, 2000) has so far not led to a significantly better match with tomography (Becker and Boschi, 2002). This implies that more realistic global, forward subduction models may be needed which include LVVs such as weakening in the mantle wedge.

Regionally, the match of mapped slab structure and predictions from slablets can be improved by more realistic solutions for the slab sinkers, or by using more detailed plate reconstructions (Bunge and Grand, 2000; Tan et al., 2002). Kárason (2002) showed that complex slab images as imaged in several subduction zones, such as the along-strike variations in the Sunda arc (Kárason and van der Hilst, 2000), may be explained by slablet modeling and prescribed trench motions. In such models, the slab is assumed to have the same viscosity as the mantle, for simplicity, $\eta' = 1$. If a dense downwelling encounters a viscosity increase, such as at 660 km, an inverted mushroom-like shape and broadening results. However, relatively large viscosity jumps of $\eta_l \gtrsim 200$ were required to reproduce the imaged broadening of the slab anomaly in the lower mantle for the Sunda arc (Kárason, 2002).

An alternative explanation for the tomographically mapped structure at reduced η_l viscosity contrasts is the folding instability of a relatively stiff slab (Ribe et al., 2007). In this case, the mantle is treated as inviscid ($\eta' \rightarrow \infty$), and only the fluid deformation of the slab is considered (e.g. Houseman and Gubbins, 1997; Ribe, 2003). Reality is somewhere between these η' -rheological endmembers, and the joint approach of Morra et al. (2006) and Capitanio et al. (2007), where the subducting lithosphere is modeled numerically by FE, and the mantle component is dealt with semi-analytically, may lead to improvements in regional models that account for the global flow contributions.

4.3.3 Lithospheric bending and partitioning of viscous dissipation

Conrad and Hager (1999a) improved on previous fluid loop analysis for subduction velocities by taking the detailed partitioning of viscous dissipation between faulted

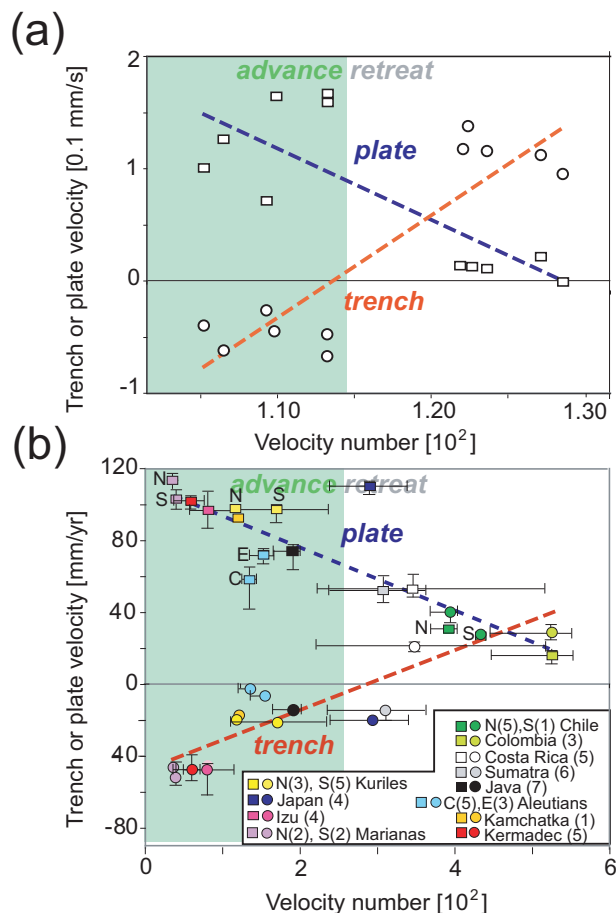


Figure 9: (a) Dependence of subducting plate velocity V_P (squares) and trench motion V_T (circles, cf. Figure 3) on “subduction velocity number”, i.e. eq. (7) normalized by a Stokes velocity (eq. 2 with $C = 1$ and $a^2 = Lh$) for the stiff ($\eta' \sim 1,000$) slab laboratory experiments of Bellahsen et al. (2005). (b) Subduction zone parameters for different trenches in nature (from Heuret and Lallemand, 2005). Legend lists color-coded trench regions with geographic subdivisions, error bars indicate the standard deviation of the mean velocities for each trench. (Figure modified from Faccenna et al., 2007, see this paper for details.)

margin, bending lithosphere, and mantle into account and tested their scaling relationships with FE computations. Such models allow exploration of the parameter space between weak and strong slab dynamics. For experiments with fixed slab bending geometry, Conrad and Hager found that a large fraction of viscous dissipation was accommodated by the bending of a viscous slab, and that a scaling relationship could be derived to predict plate velocities as a function of h , R , and η' . Becker et al. (1999) were able to fit the (exponential) rate of subduction development for different slab strengths in their dynamically evolving models as a function of η' assuming that all viscous dissipation took place in the slab. However, these authors also pointed out that this only worked if the time-dependence of R was accounted for.

Also, the type of trench motion (advancing *vs.* retreating) was shown to be affected by the buoyancy number, which measures the magnitude of slab pull relative to slab strength (Houseman and Gubbins, 1997). Becker et al. found that subducting slabs failed to develop for a system with two plates and prescribed, far-field convergence velocities for $\eta' \gtrsim 750$, consistent with the plate velocity analysis of Conrad and Hager (1999a). A tectonic application of the subduction velocity rules from Becker et al. (1999) for oceanic and continental material entering a trench was presented in Faccenna et al. (2001a). The authors argue that the subduction rates at different trench segments in the central Mediterranean can be fit with a single, simple scaling law if buoyancy variations in subducting lithosphere due to a mix of continental and oceanic lithosphere are accounted for (*cf.* Royden and Husson, 2006).

Bellahsen et al. (2005) tested the applicability of bending scaling laws further, and presented a comprehensive analysis of rollback and subduction velocities for laboratory experiments with a single, isolated slab and stiffness ratios of $\eta' \gtrsim 1000$. The dynamic behavior of such strong slabs when sinking into a layered mantle can be divided into three types: Type one always shows rollback, type two shows alternating episodes of trench rollback and advance (*cf.* Enns et al., 2005), and type three always advances (Funiciello et al., 2004). Especially the type two behavior is controlled by the interaction of the slab with the 660 km equivalent; this stage is associated with re-bending of the lithosphere at depth (*cf.* Hassani et al., 1997; Čížková et al., 2002). Such deep dynamics may be recorded geologically by means of episodic back-arc basin opening, possibly associated with different amounts of lateral flow confinement (Faccenna et al., 2001b, 2004).

Subduction is time-dependent, especially in the transient phase where the initial downwelling has not yet

reached the 660 km discontinuity. However, Bellahsen et al. (2005) were able to fit approximate steady-state behavior for fluid slabs once they have reached the ponding stage after interactions with 660 km (stage III in Figure 10a). These authors used a simplified force balance based on Conrad and Hager (1999a), neglecting any overriding-plate or fault zone terms. If parameters are measured for a certain stage of subduction, the subduction velocity

$$V' \propto \frac{\Delta\rho ghL}{(2\eta'(h/R)^3 + 3A)\eta_m} \quad (7)$$

is found to scale linearly with V_C measured from experiments (Table 1 for symbols). It is clear that the strong $(h/R)^3$ dependence will complicate application of eq. (7) to nature, and the bending geometry may be expected to vary in time and along strike.

By comparing V_{Stokes} (eq. 2) and the subduction velocity V' (eq. 7), it can be seen that the role of lithospheric viscosity (η') is modified, and typically much increased from the minor effect η' has on the Stokes velocity. In fact, V' may be normalized by a typical Stokes velocity to evaluate the role of bending and induced shear by the plate at the surface (Faccenna et al., 2007), as opposed to the vertical sinking of an isolated slab sinker. We will call V' from eq. (7) a “modified Stokes” velocity to emphasize the role of the (age-dependent) slab pull ($\Delta\rho$ type terms).

Bellahsen et al. (2005) and Funiciello et al. (2008) analyze how forces are partitioned between the lithospheric bending and mantle flow components ($(h/R)^3\eta'$ and $3A$ terms in eq. (7), respectively). In accord with the earlier work, they find that the dominant control is the bending of the lithosphere for most settings. This view of subduction dynamics where relatively strong slabs are an important control on plate velocities also finds support in the analysis of Buffett and Rowley (2006) who show that the direction of certain plate motions may be a consequence of the bending force balance. However, the Bellahsen et al. (2005) results are different from the analysis by Stegman et al. (2006), and at odds with conclusions by Schellart (2004b). Most of the discrepancies of published studies are likely due to different parameter choices with respect to slab stiffness. The division of viscous dissipation is expected to depend strongly on the rheology of the slab at the trench, which is poorly known in nature.

Dynamically evolving slabs may adjust into a minimum viscous dissipation configuration by modifying the bending geometry and the relative rate of trench motion (Enns et al., 2005). Recent work on the partitioning of viscous dissipation in dynamically evolving subduction models based on 3-D modeling as in Figure 8 indicates

that between 40 and 50% (retreating or advancing slab, respectively) may be due to bending (Di Giuseppe et al., 2008). We conclude that bending may not be the sole, dominant source of dissipation, but it is likely of great importance. The broader implication is that plate tectonics may be more strongly affected by lithospheric strength as would be expected from an isoviscous convecting system. However, the heat flow scalings suggested by Conrad and Hager (1999b) and Korenaga (2003) may overestimate the role of the lithosphere, as they are based on constant bending geometries.

4.4 Different modes of trench migration: retreat and advance

The other component of viscous dissipation, due to the induced flow in the mantle, is divided into a poloidal part similar to that of a Stokes sinker, and toroidal flow associated with trench migration (Garfunkel et al., 1986) and vortex-like motion around the slab (Buttles and Olson, 1998; Kincaid and Griffith, 2003; Funicello et al., 2004, 2006; Schellart, 2004a; Piromallo et al., 2006).

4.4.1 Toroidal flow and the role of slab width

Like lithospheric bending, toroidal flow depends on rheology, and the toroidal to poloidal flow ratio may be used to judge the character of theoretical convection models compared to observed surface velocities. For regional subduction models, the decomposition of the velocity fields can be useful to understand the temporal evolution of slab sinking into the upper mantle. While large values of toroidal flow are reported (“95-100% of the mantle flux”; Schellart et al., 2007), such statements apply only to restricted layers of the upper mantle during strong rollback. It is also best to distinguish between amplitudes of divergence and vorticity, as opposed to poloidal and toroidal velocity decompositions (*e.g.* Tackley, 2000b). The latter are preferred, and reported here.

From analysis of subduction models such as those shown in Figure 8, we find that TPRs are highly time-dependent, particularly for “free ridge” models that lack a pronounced, steady-state rollback phase (Figure 10). Mean TPR ratios are of the order of 0.5–0.9 for $\eta' = 500$ when spatially averaged over the model domain, where the high values result from fixed ridge setups where rollback is required (*cf.* Enns et al., 2005). Such overall TPR values can be compared with detailed tests for single slab snapshots by Piromallo et al. (2006). For their example geometry (similar to phase II of Figure 10a), Piromallo et al. showed that toroidal flow itself increases with slab width W . However the TPR does not depend strongly on

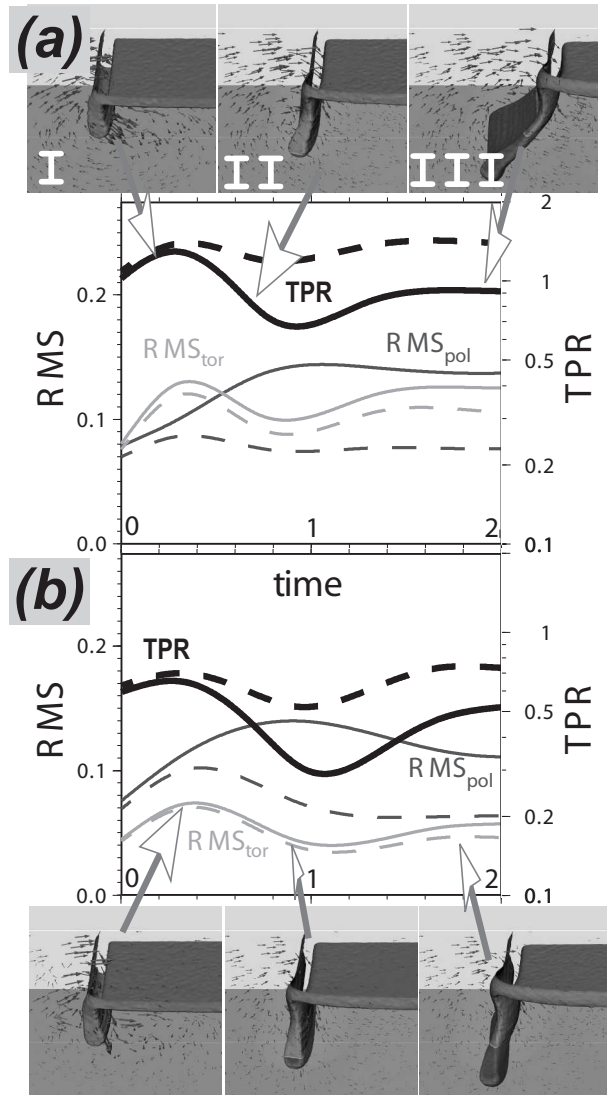


Figure 10: Temporal evolution of poloidal (dark gray) and toroidal (light gray) velocity RMS, and TPR ratio (heavy black line) for the whole domain (solid) and the upper mantle only (dashed lines). We show results for a “fixed ridge” model (a, as in Figure 8) and for a “free ridge” where the plate can advance freely (b, as in Figure 12; *cf.* Enns et al., 2005). Non-dimensional units, unity time corresponds to ~ 15 Ma, and small plots show snapshots at the indicated times as in Figure 8.

W , but increases with η' , from 0 at $\eta' = 1$ to ~ 0.5 for $\eta' = 100$, saturating at ~ 0.7 for $\eta' \gtrsim 1000$. If mantle circulation could be constrained for subduction settings independently, *e.g.* from seismic anisotropy, this relationship may be used to arrive at an indirect constraint for η' .

While TPR ratios are a kinematic construct, the toroidal flow component does allow evaluating the dynamic pressure components induced by rollback, and Royden and Husson (2006) present an analytical estimate of this flow component. Rollback pressure is expected to increase $\propto W$. This would imply that rollback rates, V_T , may scale inversely with W , as suggested by Dvorkin et al. (1993) and found in the laboratory experiments of Bellahsen et al. (2005). Consistently, Stegman et al. (2006) were able to parametrize V_T in their numerical models with a completely yielded trench region by poloidal and toroidal viscous dissipation in the mantle as a function of W , and also found that $V_T \propto 1/W$. In an application of their experiments, Schellart et al. (2007) point out that both rollback velocities and trench curvature in nature may be controlled by slab width. Narrow slabs such as the Scotia arc show fast rollback and convex trench shapes. Wide slabs such as in the Chilean roll back slowly or are stationary (Figure 4), while their trenches form concave geometries with a possible stagnation point in the center (*cf.* Russo and Silver, 1994). However, both Stegman et al.'s (2006) and Schellart et al.'s (2007) results are out of scale for V_P , which is \sim one order of magnitude lower than the observed plate velocities. This may overestimate the role of V_T for subduction zone dynamics.

4.4.2 Regional subduction dynamics and plate advance

The work by Bellahsen et al. (2005) shows that certain parameters can be used to roughly predict overall convergence V_C based on V' (eq. 7), while the partitioning into V_T and V_P remains somewhat elusive. It is possible that rollback settings follow a minimum viscous dissipation principle where a balance between the Stokes-sinker flow, the shear of the plate at the surface, and the rollback-induced shear is found (Enns et al., 2005). While several groups are working on tests of this suggestion at present, a consensus or comprehensive theoretical description has yet to emerge.

However, from an empirical point of view, Faccenna et al. (2007) showed that trends exist in the subduction velocity scaling of Bellahsen et al. (2005). Trench migration, V_T , scales inversely with plate velocity, V_P . Since $V_S = V_T + V_P$ (Figure 3), this implies that there is an anchoring effect with externally controlled V_S , similar to the results by Heuret et al. (2007) for back-arc deformation

(sec. 4.3.1). Expressed as a function of predicted subduction velocity V' , trench motion, V_T , is found to increase, and plate velocity V_P to decrease, with increasing V' in the laboratory experiments (Figure 9a). Thus, an increased subduction tendency as measured by V' (or its normalized version, the subduction velocity number of Figure 9) is converted into increased rollback V_T because of anchoring. Interestingly, similar scalings for V_T , V_P , and V' are also found for subduction zones in nature (Figure 9b). While there is large scatter, Faccenna et al. (2007) show that regional subduction zone parameters (from Heuret and Lallemand, 2005, based on HS-3) and the empirical relationships of Figure 9 can adequately predict the trench-normal components of V_P and V_T .

Issues with applying the simplified Faccenna et al. (2007) results to nature were discussed extensively in their paper. For example, we would expect regions without complications from mantle wind, and those without continental material entering the trench, to behave most closely to what is expected based on models with a single subducting plate. The Sunda arc, and as a consequence the Australian plate, are accordingly not matched well, while other subduction zones are matched better. However, Figure 11 provides a global test of the regional dynamics analysis of Faccenna et al. We computed rigid plate motions for the Australian, Pacific, and Nazca plate based on least-squares estimates of the Euler vector that best matches the trench-normal, local velocities from Faccenna et al. (2007). It is apparent that the overall motions of the major oceanic plates that have subduction zones attached can be fit by the scaling relations that were derived from isolated, highly idealized subduction models without an overriding plate.

Part of this perhaps surprising result is due to the prescribed plate geometries and the correspondingly highly correlated driving torques (Figure 5). While global models with viscous coupling at the base can predict plate motions well (Figure 6), pulling at the right plate boundaries can also, expectedly, provide a good match. However, it is intriguing that roughly the right amplitudes of HS-3 V_P values are predicted, given that this plate model includes net rotations. This implies that regional slab dynamics may indeed be invoked to excite net rotations. At first this may seem counter intuitive, but given the possible strong effect of the slabs that are attached to the plates forming the Pacific basin, this finding deserves further study beyond the preliminary global tests that were discussed in sec. 3.5.

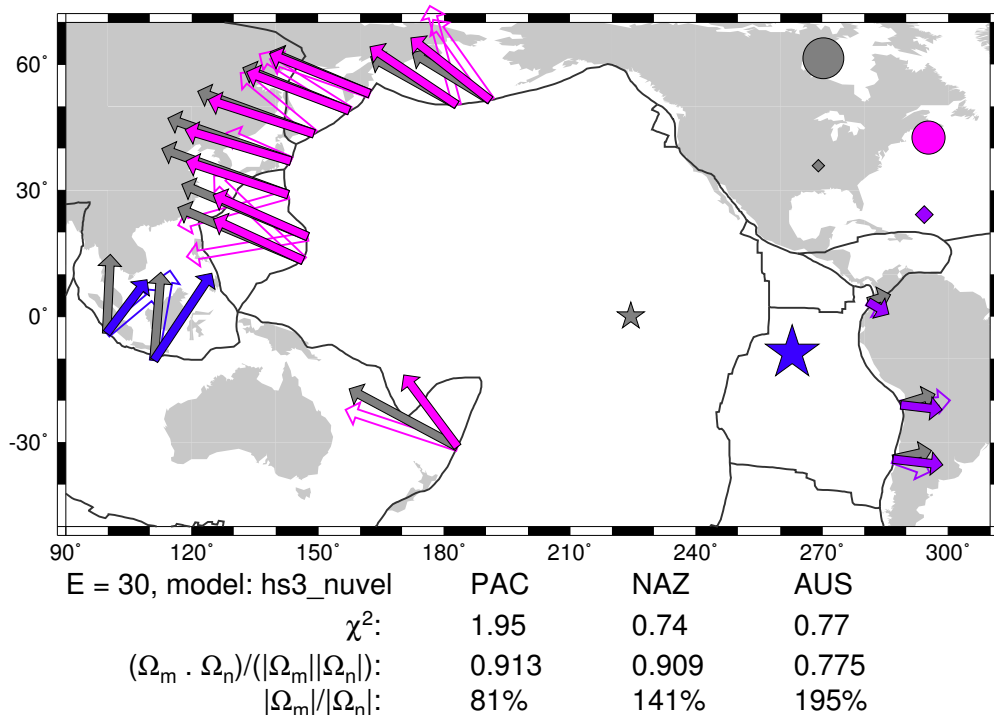


Figure 11: Best-fit plate motions (solid colored vectors) for rigid-plate Euler vectors based on matching the trench-normal velocity predictions of Faccenna et al. (2007) (open solid vectors), compared with HS-3 NUVEL (gray vectors, in the hotspot reference-frame). We allow for an azimuth error of the estimated trench segment normals of 30° before computing Euler poles (star: Australian plate; circle: Pacific; diamond: Nazca). Numbers below plot indicate χ^2 misfit, normalized correlation of Euler vectors ($(\Omega_m \cdot \Omega_n) / (|\Omega_m| |\Omega_n|)$) and amplitude ratio ($|\Omega_m| / |\Omega_n|$, values larger than unity meaning over-prediction of amplitudes).

4.4.3 Roll of slab strength for roll back

We had emphasized earlier that slab behavior in regional subduction experiments depends strongly on the viscosity of the slab η' , particularly in the trench region. The strong and weak slab experiments by Bellahsen et al. (2005) and Stegman et al. (2006), respectively, are two endmember cases. Funicello et al. (2008) therefore conducted additional experiments and were able to map out subduction behavior as a function of η' and V' . Figure 12 shows that models in the strong slab regime ($\eta' \gtrsim 10,000$, phase space “C”), on the one hand, are observed to always roll back. This is because the viscous bending is dominant, very little in-slab deformation and stretching occurs, and subduction prefers to minimize the deformation at the trench. In the C regime, dynamics are plate, or lithosphere, dominated. Weak slabs ($\eta' \lesssim 100$, phase space “A”), on the other hand, display little trench motion, deform internally, and form a Rayleigh-Taylor like viscous downwelling instead. In this regime, the dynamics are strongly mantle controlled.

In between the two extreme cases A and C is the more varied subduction behavior of phase space “B” where in-

creasing subduction velocity decreases V_P and increases V_T ; it is the high η' end of this range that was used by Faccenna et al. (2007) and discussed for Figure 9. Only for this intermediate η' field are models with larger subduction velocity observed to be retreating, and models with smaller subduction velocity are found to be advancing (Figure 11). While the intermediate η' regime might be interesting, it is not clear if it is relevant for nature. However, the η' ratios appear reasonable given other constraints on effective slab viscosity. Moreover, both advancing and retreating slabs are observed in nature (Figure 4b), and back-arc deformation (Heuret et al., 2007) as well as V_P and V_T subduction velocities (Faccenna et al., 2007) follow trends that can be explained based on isolated slab experiments in this stiffness regime. The joint match of back-arc deformation and V_T is encouraging given that plate velocities (V_P) with moderate NR can be explained with global flow models (Figures 2 and 6) without a refined representation of regional slab dynamics.

We therefore assume that viscous slab models are a useful means to understand global subduction kinematics, and that V_T is mainly controlled by deep slab dynamics.

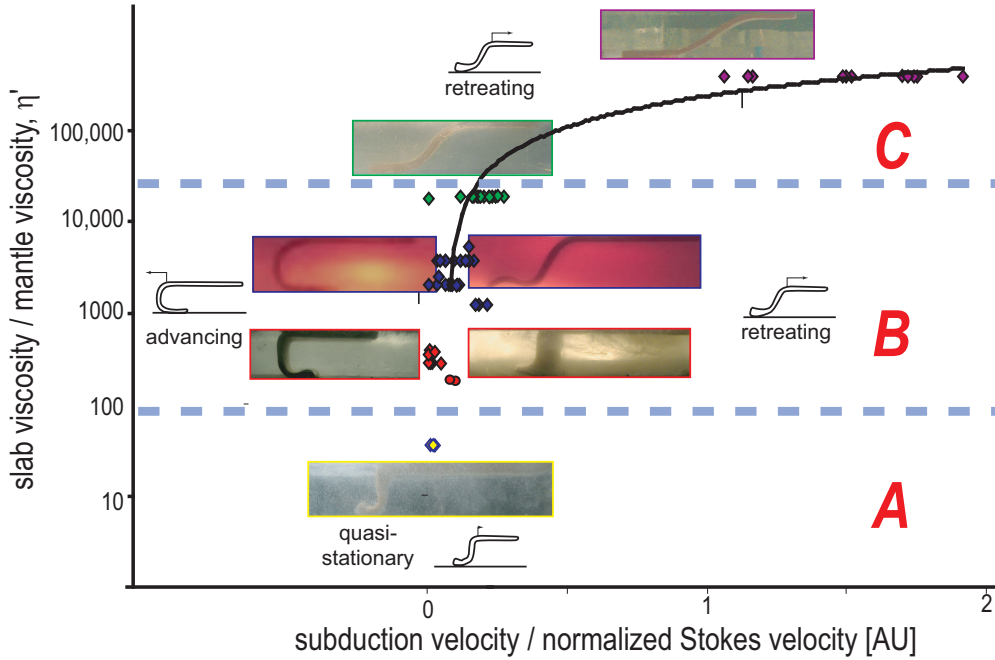


Figure 12: Laboratory model behavior for free ridge models with different slab/mantle ratios η' and normalized subduction velocities (V' of eq. 7, divided by a normalized Stokes velocity to remove the effect of buoyancy changes at constant mantle viscosity). Models are from Bellahsen et al. (2005), Funciello et al. (2008) (diamonds), and Schellart (2004b) (circles). Dashed lines are approximate divisions of model behavior; figure is modified from Funciello et al. (2008).

One can then turn the argument around and explore the inverse correlation between V_T and V_P as a function of η' and reference frames. Funciello et al. (2008) summarize existing, and conduct new, free trailing-edge subduction models with an isolated viscous slab (Figure 12). They show that the correlation between the two kinematic parameters holds for experiments with a range of η' within the intermediate field of Figure 12. The best-fit slope $\alpha = V_T/V_P$ is found to increase from $\alpha \sim 0.5$ at $\eta' \sim 100$ to $\alpha \sim 1.75$ at $\eta' \sim 15,000$. In nature, the strength of the anti-correlation between V_P and V_T and the amplitude of α depend on the reference frame (Figure 4); α varies from ~ 0.25 for NNR to ~ 0.75 for HS-3 (Funciello et al., 2008).

Therefore, none of the α slopes for largest η' are observed in nature, as trench motion is usually smaller than plate velocities. Instead, the observed α values may indicate that slabs are relatively weak, with compatible η' values between ~ 150 and ~ 350 (Funciello et al., 2008). Using this line of reasoning, the experiments by Bellahsen et al. (2005) were probably conducted at η' values that are too high, and the inviscid fluid models of, *e.g.*, Shemenda (1994) and Houseman and Gubbins (1997) with $\eta' \rightarrow \infty$ might make too drastic an assumption with regard to the neglect of mantle flow. Schellart's (2004a) experiments

are closer to the η' values that are implied by Funciello et al.'s study, but on the low end. The experiments of Schellart et al. (2007) are, however, inconsistent in that their α ratios are significantly higher than those observed in nature.

Viscosity ratios η' of the order of 100, as expected given the arguments above, are also consistent with arguments about subductability of fluid slabs (Conrad and Hager, 1999a; Becker et al., 1999), the geopotential and in-slab force transmission (Moresi and Gurnis, 1996; Zhong and Davies, 1999), as well as the flexure study of Billen and Gurnis (2005). A range of observations therefore indicate that subducting oceanic lithosphere behaves as a viscous fluid that is effectively ~ 500 times stiffer than the upper mantle. Is an effective viscosity a meaningful concept? In reality, temperature- and pressure-dependent diffusion and dislocation creep mechanisms control slab deformation, along with plastic yielding mechanisms that will limit maximum deviatoric stresses (Kirby and Kronenberg, 1987; Riedel and Karato, 1997; Hirth and Kohlstedt, 2004). Even for olivine, several creep law parameters are not well measured (*e.g.* activation volume), constrained (*e.g.* volatile content), or may dynamically evolve (*e.g.* grain size) in nature. However, several authors have studied which visco-plastic olivine-

type rheologies lead to “slab-like” subduction in the upper mantle. Geodynamic models for the present-day potential temperatures (*e.g.* Tetzlaff and Schmeling, 2000; van Hunen et al., 2000; Billen and Hirth, 2007), and the Earth’s past (van Hunen and van den Berg, 2007) have been explored. From these experiments, it is apparent that both slab shapes and average viscosities are dynamically evolving. However, η' values of $\sim 10^4 \dots 10^5$ for the slab outside the trench are plausible, along with significant weakening toward the trench, down to $\eta' \sim 10^2 \dots 10^3$. Lab-derived rheologies in thermo-mechanical models are thus consistent with the range of η' used in the simplified models here.

5 Conclusions

Plate kinematics may be understood by the dynamical behavior of fluid slabs sinking into a mantle that is viscously stratified. Regional modeling indicates that roll-back, trench curvature, and back-arc deformation are consistent with slabs that are ~ 250 to 500 times stiffer than the mantle, in terms of the effective viscosity in the trench region. The dynamics are controlled by bending, mantle drag, and interactions with the higher viscosity lower mantle.

The net rotation of the lithosphere may be caused jointly by regional slab dynamics, buoyant upwellings, and the effect of continental keels, although global models based on slabs alone were not found to be effective in inducing net rotations as large as those of recent hotspot models. However, such global models with weak zones and other lateral viscosity variations lead to a good fit with regard to other plate tectonic scores such as intra-plate deformation, and oceanic to continental plate velocity ratios.

While much progress has been made, several important issues such as the physics of the partitioning between roll-back and subducting plate velocity over time are still not fully resolved. It is also clear that conclusions about subduction dynamics are somewhat dependent on the choice of the plate kinematic model and assumptions about slab rheology. This is a problem, as the strength of the slab is poorly constrained from either large-scale modeling inferences or laboratory measurements.

It appears crucial to improve the weak zone and plate boundary implementation in global subduction models. A more sophisticated rheological treatment of slabs in global flow may also improve the match between geodynamic forward models and seismic tomography. Moreover, advances in the plate boundary treatment will help to evaluate the role of the upper mechanical boundary condition for numerical models, and to perform truly quanti-

tative comparisons between laboratory analog models and numerics.

Most of the results discussed in this review indicate that the role of the overriding plate may be small for controlling subduction dynamics. However, this also needs to be evaluated with joint lithospheric-mantle models, particularly in the context of a thick, continental overriding plate.

Acknowledgments

Discussions during the SUBCO meeting in Montpellier in June 2007 helped to distill some of the ideas summarized here. We thank our reviewers Saskia Goes and Carolina Lithgow-Bertelloni as well as F. Funiciello, M. I. Billen, B. J. P. Kaus, and S. D. King for comments on an earlier version of this manuscript. In addition, we thank A. Heuret and F. Funiciello for sharing their data, and S. Zhong and L. Moresi for their computer software. Computations were conducted at the University of Southern California Center for High Performance Computing and Communications (www.usc.edu/hpcc), and we used software from CIG (geodynamics.org). Most figures were produced with the GMT software by Wessel and Smith (1991). This research was supported by NSF grants EAR-0643365 and 0451952.

References

- Batchelor GK (1967) An introduction to fluid dynamics. Cambridge University Press, Cambridge UK
- Becker TW (2006) On the effect of temperature and strain-rate dependent viscosity on global mantle flow, net rotation, and plate-driving forces. *Geophys J Int* 167:943–957
- Becker TW (2008) Azimuthal seismic anisotropy constrains net rotation of the lithosphere. *Geophys Res Lett* 35, doi:10.1029/2007GL032928, correction: doi:10.1029/2008GL033946
- Becker TW, Boschi L (2002) A comparison of tomographic and geodynamic mantle models. *Geochemistry Geophysics Geosystems* 3, 2001GC000168
- Becker TW, Faccenna C, O’Connell RJ, Giardini D (1999) The development of slabs in the upper mantle: insight from numerical and laboratory experiments. *J Geophys Res* 104:15207–15225
- Becker TW, Kellogg JB, Ekström G, O’Connell RJ (2003) Comparison of azimuthal seismic anisotropy from

- surface waves and finite-strain from global mantle-circulation models. *Geophys J Int* 155:696–714
- Becker TW, O’Connell RJ (2001) Predicting plate velocities with geodynamic models. *Geochemistry Geophysics Geosystems* 2, 2001GC000171
- Becker TW, Schulte-Pelkum V, Blackman DK, Kellogg JB, O’Connell RJ (2006) Mantle flow under the western United States from shear wave splitting. *Earth Planet Sci Lett* 247:235–251
- Bellahsen N, Faccenna C, Funiciello F (2005) Dynamics of subduction and plate motion in laboratory experiments: insights into the plate tectonics behavior of the Earth. *J Geophys Res* 110, doi:10.1029/2004JB002999
- Bercovici D (2003) The generation of plate tectonics from mantle convection. *Earth Planet Sci Lett* 205:107–121
- Bercovici D, Ricard Y, Richards M (2000) The relationship between mantle dynamics and plate tectonics: a primer. In: Richards M, Gordon R, van der Hilst RD (eds.), *The History and Dynamics of Global Plate Motions*, American Geophysical Union, Washington, DC, vol. 121 of *Geophysical Monograph*, 5–46
- Bevis M (1986) The curvature of Wadati-Benioff zones and the torsional rigidity of subducting plates. *Nature* 323:52–53
- Bevis M (1988) Seismic slip and down dip strain rate in Wadati-Benioff zones. *Science* 240:1317–1319
- Billen MI (2008) Modeling the dynamics of subducting slabs. *Ann Rev Earth Planet Sci* 36:325–356
- Billen MI, Gurnis M (2001) A low viscosity wedge in subduction zones. *Earth Planet Sci Lett* 193:227–236
- Billen MI, Gurnis M (2003) Multiscale dynamics of the Tonga-Kermadec subduction zone. *Geophys J Int* 153:359–388
- Billen MI, Gurnis M (2005) Constraints on subducting plate strength within the Kermadec trench. *J Geophys Res* 110, doi:10.1029/2004JB003308
- Billen MI, Hirth G (2007) Rheologic controls on slab dynamics. *Geochemistry Geophysics Geosystems* 8, doi:10.1029/2007GC001597:Q08012
- Bird P (2003) An updated digital model of plate boundaries. *Geochemistry Geophysics Geosystems* 4, doi:10.1029/2001GC000252
- Boschi L, Becker TW, Steinberger B (2007) Mantle plumes: dynamic models and seismic images. *Geochemistry Geophysics Geosystems* 8, Q10006, doi:10.1029/2007GC001733
- Brace WF, Kohlstedt DL (1980) Limits on lithospheric stress imposed by laboratory experiments. *J Geophys Res* 85:6248–6252
- Budiansky R, Carrier GF (1973) The pointless wedge. *SIAM J Appl Mech* 25:378–387
- Buffett BA, Rowley DB (2006) Plate bending at subduction zones: Consequences for the direction of plate motions. *Earth Planet Sci Lett* 245:359–364
- Bunge HP, Grand SP (2000) Mesozoic plate-motion history below the northeast Pacific Ocean from seismic images of the subducted Farallon slab. *Nature* 405:337–340
- Burov EB, Diament M (1995) The effective elastic thickness (T_e) of continental lithosphere: What does it really mean? *J Geophys Res* 100:3905–3927
- Buttles J, Olson P (1998) A laboratory model of subduction zone anisotropy. *Earth Planet Sci Lett* 164:245–262
- Byerlee J (1978) Friction of rock. *Pure Appl Geophys* 116:615–626
- Čadek O, Fleitout L (2003) Effect of lateral viscosity variations in the top 300 km of the mantle on the geoid and dynamic topography. *Geophys J Int* 152:566–580
- Čadek O, Ricard Y, Martinec Z, Matyska C (1993) Comparison between Newtonian and non-Newtonian flow driven by internal loads. *Geophys J Int* 112:103–114
- Capitanio FA, Morra G, Goes S (2007) Dynamic models of downgoing plate-buoyancy driven subduction: Subduction motions and energy dissipation. *Earth Planet Sci Lett* 262:284–297
- Carlson RL, Melia PJ (1984) Subduction hinge migration. *Tectonophysics* 102:1–16
- Chapple WM, Tullis TE (1977) Evaluation of the forces that drive the plates. *J Geophys Res* 82:1967–1984
- Chase CG (1978) Extension behind island arcs and motion relative to hot spots. *J Geophys Res* 83:5385–5387
- Chen J, King SD (1998) The influence of temperature and depth dependent viscosity on geoid and topography profiles from models of mantle convection. *Phys Earth Planet Inter* 106:75–91

- Christensen U (2001) Geodynamic models of deep subduction. *Phys Earth Planet Inter* 127:25–34
- Christensen UR (1996) The influence of trench migration on slab penetration into the lower mantle. *Earth Planet Sci Lett* 140:27–39
- Christensen UR, Yuen DA (1984) The interaction of a subducting lithospheric slab with a chemical or phase boundary. *J Geophys Res* 89:4389–4402
- Čížková H, Čadek O, Slancová A (1998) Regional correlation analysis between seismic heterogeneity in the lower mantle and subduction in the last 180 Myr: implications for mantle dynamics and rheology. *Pure Appl Geophys* 151:527–537
- Čížková H, van Hunen J, van den Berg AP, Vlaar NJ (2002) The influence of rheological weakening and yield stress on the interaction of slabs with the 670-km discontinuity. *Earth Planet Sci Lett* 199:447–457
- Clift P, Vannucchi P (2004) Controls on tectonic accretion versus erosion in subduction zones: Implications for the origin and recycling of the continental crust. *Rev Geophys* 42, RG2001:1–31
- Conrad CP, Bilek S, Lithgow-Bertelloni C (2004) Great earthquakes and slab-pull: Interaction between seismic coupling and plate-slab coupling. *Earth Planet Sci Lett* 218:109–122
- Conrad CP, Hager BH (1999a) The effects of plate bending and fault strength at subduction zones on plate dynamics. *J Geophys Res* 104:17551–17571
- Conrad CP, Hager BH (1999b) The thermal evolution of an Earth with strong subduction zones. *Geophys Res Lett* 26:3041–3044
- Conrad CP, Lithgow-Bertelloni C (2002) How mantle slabs drive plate tectonics. *Science* 298:207–209
- Conrad CP, Lithgow-Bertelloni C (2004) The temporal evolution of plate driving forces: Importance of “slab suction” versus “slab pull” during the Cenozoic. *J Geophys Res* 109, doi:10.1029/2004JB002991
- Conrad CP, Lithgow-Bertelloni C (2006) Influence of continental roots and asthenosphere on plate-mantle coupling. *Geophys Res Lett* 33, doi:10.1029/2005GL02562
- Cruciani C, Carminati E, Doglioni C (2005) Slab dip vs. lithosphere age: no direct function. *Earth Planet Sci Lett* 238:298–310
- Davies GF (1995) Penetration of plates and plumes through the mantle transition zone. *Earth Planet Sci Lett* 133:507–516
- DeMets C, Gordon RG, Argus DF, Stein S (1994) Effect of recent revisions to the geomagnetic reversal time scale on estimates of current plate motions. *Geophys Res Lett* 21:2191–2194
- Deparis V, Legros H, Ricard Y (1995) Mass anomalies due to subducted slabs and simulations of plate motion since 200 My. *Earth Planet Sci Lett* 89:271–280
- Di Giuseppe E, van Hunen J, Funicello F, Faccenna C, Giardini D (2008) Slab stiffness controls trench motion: insights from numerical models. *Geochemistry Geophysics Geosystems* 9, doi:10.1029/2007GC001776:Q02014
- Doglioni C (1990) The global tectonic pattern. *J Geodynamics* 12:21–38
- Doglioni C, Carminati E, Cuffaro M, Scrocca D (2007) Subduction kinematics and dynamic constraints. *Earth Sci Rev* 83:125–175
- Dumoulin C, Bercovici D, Wessel P (1998) A continuous plate-tectonic model using geophysical data to estimate plate-margin widths, with a seismicity-based example. *Geophys J Int* 133:379–389
- Dvorkin J, Nur A, Mavko G, Ben-Avraham Z (1993) Narrow subducting slabs and the origin of backarc basins. *Tectonophysics* 227:63–79
- Dziewoński AM, Anderson DL (1981) Preliminary reference Earth model. *Phys Earth Planet Inter* 25:297–356
- England PC, Molnar P (1997) Active deformation of Asia: from kinematics to dynamics. *Science* 278:647–650
- Enns A, Becker TW, Schmeling H (2005) The dynamics of subduction and trench migration for viscosity stratification. *Geophys J Int* 160:761–775
- Faccenna C, Becker TW, Lucente FP, Jolivet L, Rossetti F (2001a) History of subduction and back-arc extension in the central Mediterranean. *Geophys J Int* 145:809–820
- Faccenna C, Davy P, Brun JP, Funicello R, Giardini D, Mattei M, Nalpas T (1996) The dynamics of back-arc extension: an experimental approach to the opening of the Tyrrhenian Sea. *Geophys J Int* 126:781–795

- Faccenna C, Funicello F, Giardini D, Lucente P (2001b) Episodic back-arc extension during restricted mantle convection in the Central Mediterranean. *Earth Planet Sci Lett* 187:105–116
- Faccenna C, Giardini D, Davy P, Argentieri A (1999) Initiation of subduction at Atlantic type margins: Insights from laboratory experiments. *J Geophys Res* 104:2749–2766
- Faccenna C, Heuret A, Funicello F, Lallemand S, Becker TW (2007) Predicting trench and plate motion from the dynamics of a strong slab. *Earth Planet Sci Lett* 257:29–36
- Faccenna C, Piromallo C, Crespo Blanc A, Jolivet L, Rossetti F (2004) Lateral slab deformation and the origin of the arcs of the western Mediterranean. *Tectonics* 23, doi:10.1029/2002TC001488:TC1012
- Fischer KM, Jordan TH (1991) Seismic strain rate and deep slab deformation in Tonga. *J Geophys Res* 96:14429–14444
- Forsyth DW, Uyeda S (1975) On the relative importance of the driving forces of plate motion. *Geophys J R Astr Soc* 43:163–200
- Forte A, Peltier WR (1994) The kinematics and dynamics of poloidal-toroidal coupling in mantle flow: the importance of surface plates and lateral viscosity variations. *Adv Geophys* 36:1–119
- Forte AM, Mitrovica JX (2001) Deep-mantle high-viscosity flow and thermochemical structure inferred from seismic and geodynamic data. *Nature* 410:1049–1056
- Forte AM, Peltier WR (1987) Plate tectonics and aspherical earth structure: the importance of poloidal-toroidal coupling. *J Geophys Res* 92:3645–3679
- Funicello F, Faccenna C, Giardini D (2004) Flow in the evolution of subduction system: Insights from 3-D laboratory experiments. *Geophys J Int* 157:1393–1407
- Funicello F, Faccenna C, Giardini D, Regenauer-Lieb K (2003a) Dynamics of retreating slabs (part 2): insights from 3D laboratory experiments. *J Geophys Res* 108, doi:10.1029/2001JB000896
- Funicello F, Faccenna C, Heuret A, Di Giuseppe E, Lallemand S, Becker TW (2008) Trench migration, net rotation and slab-mantle coupling. *Earth Planet Sci Lett* 271:233–240
- Funicello F, Moroni M, Piromallo C, Faccenna C, Cenedese A, Bui HA (2006) Mapping flow during retreating subduction: laboratory models analyzed by Feature Tracking. *J Geophys Res* 111, doi:10.1029/2005JB003792
- Funicello F, Morra G, Regenauer-Lieb K, Giardini D (2003b) Dynamics of retreating slabs (part 1): insights from numerical experiments. *J Geophys Res*
- Gable CW, O’Connell RJ, Travis BJ (1991) Convection in three dimensions with surface plates: generation of toroidal flow. *J Geophys Res* 96:8391–8405
- Garfunkel Z, Anderson CA, Schubert G (1986) Mantle circulation and the lateral migration of subducted slabs. *J Geophys Res* 91:7205–7223
- Giardini D, Woodhouse JH (1984) Deep seismicity and modes of deformation in Tonga subduction zone. *Nature* 307:505–509
- Giardini D, Woodhouse JH (1986) Horizontal shear flow in the mantle beneath the Tonga arc. *Nature* 319:551–555
- Gordon RG (2000) Diffuse oceanic plate boundaries: Strain rates, vertically averaged rheology, and comparisons with narrow plate boundaries and stable plate interiors. In: Richards MA, Gordon RG, van der Hilst RD (eds.), *The History and Dynamics of Global Plate Motion*, American Geophysical Union, Washington DC, vol. 121 of *Geophysical Monograph*, 143–159
- Gordon RG, Jurdy DM (1986) Cenozoic global plate motions. *J Geophys Res* 91:12389–12406
- Gouillou-Frottier L, Buttles J, Olson P (1995) Laboratory experiments on the structure of subducted lithosphere. *Earth Planet Sci Lett* 133:19–34
- Grand SP, van der Hilst RD, Widiyantoro S (1997) Global seismic tomography; a snapshot of convection in the Earth. *GSA Today* 7:1–7
- Griffiths RW, Hackney RI, van der Hilst RD (1995) A laboratory investigation of effects of trench migration on the descent of subducted slabs. *Earth Planet Sci Lett* 133:1–17
- Gripp AE, Gordon RG (1990) Current plate velocities relative to the hotspots incorporating the NUVEL-1 global plate motion model. *Geophys Res Lett* 17:1109–1112
- Gripp AE, Gordon RG (2002) Young tracks of hotspots and current plate velocities. *Geophys J Int* 150:321–361

- Gudmundsson O, Sambridge M (1998) A regionalized upper mantle (RUM) seismic model. *J Geophys Res* 103:7121–7136
- Gurnis M, Davies GF (1986) The effect of depth-dependent viscosity on convective mixing in the mantle and the possible survival of primitive mantle. *Geophys Res Lett* 13:541–544
- Gurnis M, Hager BH (1988) Controls of the structure of subducted slabs. *Nature* 335:317–321
- Gurnis M, Zhong S, Toth J (2000) On the competing roles of fault reactivation and brittle failure in generating plate tectonics from mantle convection. In: Richards MA, Gordon RG, van der Hilst RD (eds.), *The History and Dynamics of Global Plate Motions*, AGU, Washington DC, vol. 121 of *Geophysical Monograph*, 73–94
- Hager BH (1984) Subducted slabs and the geoid: constraints on mantle rheology and flow. *J Geophys Res* 89:6003–6015
- Hager BH, Clayton RW (1989) Constraints on the structure of mantle convection using seismic observations, flow models, and the geoid. In: Peltier WR (ed.), *Mantle convection: Plate tectonics and global dynamics*, Gordon and Breach Science Publishers, New York, NY, vol. 4 of *The Fluid Mechanics of Astrophysics and Geophysics*, 657–763
- Hager BH, O’Connell RJ (1978) Subduction zone dip angles and flow derived by plate motion. *Tectonophysics* 50:111–133
- Hager BH, O’Connell RJ (1981) A simple global model of plate dynamics and mantle convection. *J Geophys Res* 86:4843–4867
- Hager BH, O’Connell RJ, Raefsky A (1983) Subduction, back-arc spreading and global mantle flow. *Tectonophysics* 99:165–189
- Hall CE, Gurnis M (2005) Strength of fracture zones from their barymetric and gravitational evolution. *J Geophys Res* 110, doi:10.1029/2004JB003312
- Hall CE, Gurnis M, Sdrolias M, Lavier LL, Muller RD (2003) Catastrophic initiation of subduction following forced convergence at transform boundaries. *Earth Planet Sci Lett* 212:15–30
- Han L, Gurnis M (1999) How valid are dynamical models of subduction and convection when plate motions are prescribed? *Phys Earth Planet Inter* 110:235–246
- Hassani R, Jongmans D, Chéry J (1997) Study of plate deformation and stress in subduction processes using two-dimensional numerical models. *J Geophys Res* 102:17951–17965
- Heuret A, Funicello F, Faccenna C, Lallemand S (2007) Plate kinematics, slab shape and back-arc stress: A comparison between laboratory models and current subduction zones. *Earth Planet Sci Lett* 256:473–483
- Heuret A, Lallemand S (2005) Slab dynamics and back-arc deformation. *Phys Earth Planet Inter* 149:31–51
- Hirth G, Kohlstedt DL (2004) Rheology of the upper mantle and the mantle wedge: A view from the experimentalists. In: Eiler J (ed.), *Inside the Subduction Factory*, American Geophysical Union, Washington DC, vol. 138 of *Geophysical Monograph*, 83–105
- Holt WE (1995) Flow fields within the Tonga slab determined from the moment tensors of deep earthquakes. *Geophys Res Lett* 22:989–992
- Houseman GA, Gubbins D (1997) Deformation of subducted oceanic lithosphere. *Geophys J Int* 131:535–551
- Humphreys ED, Coblenz D (2007) North American dynamics and western U.S. tectonics. *Rev Geophys* 45, RG3001:doi:10.1029/2005RG000181
- Husson L, Conrad CP, Faccenna C (2007) Tethyan closure, Andean orogeny, and the westward drift of the Pacific basin. *Earth Planet Sci Lett* submitted
- Husson L, Ricard Y (2004) Stress balance above subduction: application to the Andes. *Earth Planet Sci Lett* 222:1037–1050
- Iaffaldano G, Bunge HP, Dixon TH (2006) Feedback between mountain belt growth and plate convergence. *Geology* 34:893–896
- Isacks B, Molnar P (1971) Distribution of stresses in the descending lithosphere from a global survey of focal-mechanism solutions of mantle earthquakes. *Rev Geophys Space Phys* 9:103–175
- Ita J, King SD (1998) The influence of thermodynamic formulation on simulations of subduction zone geometry and history. *Geophys Res Lett* 25:1463–1466
- Jacoby WR, Schmeling H (1981) Convection experiments and driving mechanism. *Geol Rundschau* 24:217–284
- Jarrard RD (1986) Relations among subduction parameters. *Rev Geophys* 24:217–284

- Jordan TH (1978) Composition and development of the continental tectosphere. *Nature* 274:544–548
- Káráson H (2002) Constraints on mantle convection from seismic tomography and flow modeling. Ph.D. thesis, Massachusetts Institute of Technology, Cambridge MA
- Káráson H, van der Hilst RD (2000) Constraints on mantle convection from seismic tomography. In: Richards MA, Gordon RG, van der Hilst RD (eds.), *The History and Dynamics of Global Plate Motion*, American Geophysical Union, Washington DC, vol. 121 of *Geophysical Monograph*, 277–288
- Karato Si (1998) Seismic anisotropy in the deep mantle, boundary layers and the geometry of convection. *Pure Appl Geophys* 151:565–587
- Kaus BJP, Becker TW (2007) Effects of elasticity on the Rayleigh-Taylor instability: implications for large-scale geodynamics. *Geophys J Int* 168:843–862
- Kaus BJP, Podladchikov YY (2006) Initiation of localized shear in visco-elasto-plastic rocks. *J Geophys Res* 111, doi:10.1029/2005JB003652
- Kemp DV, Stevenson DJ (1996) A tensile, flexural model for the initiation of subduction. *Geophys J Int* 125:73–94
- Kincaid C, Griffith RW (2003) Laboratory models of the thermal evolution of the mantle during rollback subduction. *Nature* 425:58–62
- Kincaid C, Olson P (1987) An experimental study of subduction and slab migration. *J Geophys Res* 92:13832–13840
- King SD (2001) Subduction: Observations and geodynamic models. *Phys Earth Planet Inter* 127:9–24
- King SD (2007) Mantle downwellings and the fate of subducting slabs: constraints from seismology, geoid, topography, geochemistry, and petrology. In: Schubert G, Bercovici D (eds.), *Treatise on Geophysics*, Elsevier. In press
- King SD, Gable CW, Weinstein SA (1992) Models of convection-driven tectonic plates: a comparison of methods and results. *Geophys J Int* 109:481–487
- King SD, Hager BH (1990) The relationship between plate velocity and trench viscosity in Newtonian and power-law subduction calculations. *Geophys Res Lett* 17:2409–2412
- Kirby SH, Kronenberg AK (1987) Rheology of the lithosphere: Selected topics. *Rev Geophys* 25:1219–1244
- Kley J (1999) Geologic and geometric constraints on a kinematic model of the Bolivian orocline. *J South Amer Earth Sci* 12:221–235
- Korenaga J (2003) Energetics of mantle convection and the fate of fossile heat. *Geophys Res Lett* 30, 8:doi:10.1029/2003GL016
- Kreemer C, Holt WE, Haines AJ (2003) An integrated global model of present-day plate motions and plate boundary deformation. *Geophys J Int* 154:5–34
- Lallemand S (1995) High rates of arc consumption by subduction processes: some consequences. *Geology* 23:551–554
- Lallemand S, Heuret A, Boutelier D (2005) On the relationships between slab dip, back-arc stress, upper plate absolute motion, and crustal nature in subduction zones. *Geochemistry Geophysics Geosystems* 6, doi:10.1029/2005GC000917
- Lee CTA, Lenardic A, Cooper CM, Niu F, Levander A (2005) The role of chemical boundary layers in regulating the thickness of continental and oceanic thermal boundary layers. *Earth Planet Sci Lett* 230:379–395
- Lenardic A, Moresi LN, Jellinek AM, Manga M (2005) Continental insulation, mantle cooling, and the surface area of oceans and continents. *Earth Planet Sci Lett* 234:317–333
- Lithgow-Bertelloni C, Gynn JH (2004) Origin of the lithospheric stress field. *J Geophys Res* 109, doi:10.1029/2003JB002467
- Lithgow-Bertelloni C, Richards MA (1995) Cenozoic plate driving forces. *Geophys Res Lett* 22:1317–1320
- Lithgow-Bertelloni C, Richards MA (1998) The dynamics of Cenozoic and Mesozoic plate motions. *Rev Geophys* 36:27–78
- Lithgow-Bertelloni C, Richards MA, Ricard Y, O’Connell RJ, Engebretson DC (1993) Toroidal-poloidal partitioning of plate motions since 120 Ma. *Geophys Res Lett* 20:375–378
- McAdoo DC, Martin CF, Polouse P (1985) Seasat observations of flexure: Evidence for a strong lithosphere. *Tectonophysics* 116:209–222

- McClusky S, Bassanian S, Barka A, Demir C, Ergintav S, Georgiev I, Gurkan O, Hamburger M, Hurst K, Kahle H, Kastens K, Kekelidze G, King R, Kotzev V, Lenk O, Mahmoud S, Mishin A, Nadariya M, Ouzounis A, Paradissis D, Peter Y, Preilepin M, Reilinger R, Sanli I, Seeger H, Tealeb A, Toksoz MN, Veis G (2000) Global Positioning System constraints on plate kinematics and dynamics in the eastern Mediterranean and Caucasus. *J Geophys Res* 105:5695–5719
- McKenzie DP (1969) Speculations on the consequences and causes of plate motions. *Geophys J R Astr Soc* 18:1–32
- McKenzie DP, Parker RL (1967) The North Pacific; an example of tectonics on a sphere. *Nature* 216:1276–1280
- Melosh HJ, Raefsky A (1980) The dynamical origin of subduction zone topography. *Geophys J R Astr Soc* 60:333–354
- Melosh HJ, Williams CA (1989) Mechanics of graben formation in crustal rocks: A finite element analysis. *J Geophys Res* 94:13961–13973
- Mihálffy P, Steinberger B, Schmelting H (2007) The effect of the large-scale mantle flow field on the Iceland hotspot track. *Tectonophysics* in press
- Minster JB, Jordan TH (1978) Present-day plate motions. *J Geophys Res* 83:5331–5354
- Mitrovica JX, Forte AM (2004) A new inference of mantle viscosity based upon joint inversion of convection and glacial isostatic adjustment data. *Earth Planet Sci Lett* 225:177–189
- Molnar P, Stock J (1987) Relative motions of hotspots in the Pacific, Atlantic, and Indian Oceans since Late Cretaceous time. *Nature* 327:587–591
- Moore GE (1965) Cramming more components onto integrated circuits. *Electronics* 38, 8
- Moresi LN, Dufour F, Muehlhaus HB (2002) Mantle convection modeling with viscoelastic/brittle lithosphere: numerical modeling and plate tectonic modeling. *Pure Appl Geophys* 159:2335–2356
- Moresi LN, Gurnis M (1996) Constraints on the lateral strength of slabs from three-dimensional dynamic flow models. *Earth Planet Sci Lett* 138:15–28
- Moresi LN, Solomatov V (1998) Mantle convection with a brittle lithosphere: thoughts on the global tectonic styles of the Earth and Venus. *Geophys J Int* 133:669–682
- Moresi LN, Solomatov VS (1995) Numerical investigations of 2D convection with extremely large viscosity variations. *Phys Fluids* 7:2154–2162
- Morgan JP (1971) Convection plumes in the lower mantle. *Nature* 230:42–43
- Morgan WJ (1968) Rises, trenches, great faults, and crustal blocks. *J Geophys Res* 73:1959–1982
- Morra G, Regenauer-Lieb K, Giardini D (2006) Curvature of oceanic arcs. *Geology* 34:877–880
- Moucha R, Forte AM, Mitrovica JX, Daradich A (2007) Lateral variations in mantle rheology: implications for convection related surface observables and inferred viscosity models. *Geophys J Int* 169:113–135
- Muhlhaus HB, Regenauer-Lieb K (2005) Towards a self-consistent plate mantle model that includes elasticity: simple benchmarks and application to basic modes of convection. *Geophys J Int* 163:788–800
- O’Connell RJ, Gable CW, Hager BH (1991) Toroidal-poloidal partitioning of lithospheric plate motions. In: Sabadini R, Lambeck K (eds.), *Glacial Isostasy, Sea-Level and Mantle Rheology*, Kluwer Academic Publishers, Norwell MA, 535–551
- Olbertz D, Wortel MJR, Hansen U (1997) Trench migration and subduction zone geometry. *Geophys Res Lett* 24:221–224
- Olson P, Bercovici D (1991) On the equipartitioning of kinematic energy in plate tectonics. *Geophys Res Lett* 18:1751–1754
- O’Neill C, Müller D, Steinberger B (2005) On the uncertainties in hot spot reconstructions and the significance of moving hot spot reference frames. *Geochemistry Geophysics Geosystems* 6
- Phipps Morgan J, Morgan WJ, Zhang YS, Smith WHF (1995) Observational hints for a plume-fed, suboceanic asthenosphere and its role in mantle convection. *J Geophys Res* 100:12753–12767
- Piromallo P, Becker TW, Funicello F, Faccenna C (2006) Three-dimensional instantaneous mantle flow induced by subduction. *Geophys Res Lett* 33, doi:10.1029/2005GL025390

- Ranero C, Phipps Morgan J, McIntosh K, Reichert C (2003) Bending-related faulting and mantle serpentinization at the Middle America trench. *Nature* 425:367–373
- Regenauer-Lieb K, Yuen DA, Branlund J (2001) The initiation of subduction; criticality by addition of water? *Science* 294:578–580
- Ribe NM (1992) The dynamics of thin shells with variable viscosity and the origin of toroidal flow in the mantle. *Geophys J Int* 110:537–552
- Ribe NM (2003) Periodic folding of viscous sheets. *Phys Rev E* 66, 036305
- Ribe NM, Stutzmann E, Ren Y, van der Hilst R (2007) Buckling instabilities of subducted lithosphere beneath the transition zone. *Earth Planet Sci Lett* 254:173–179
- Ricard Y, Doglioni C, Sabadini R (1991) Differential rotation between lithosphere and mantle: A consequence of lateral mantle viscosity variations. *J Geophys Res* 96:8407–8415
- Ricard Y, Richards MA, Lithgow-Bertelloni C, Le Stunff Y (1993) A geodynamic model of mantle density heterogeneity. *J Geophys Res* 98:21895–21909
- Ricard Y, Vigny C (1989) Mantle dynamics with induced plate tectonics. *J Geophys Res* 94:17543–17559
- Richards MA (1991) Hotspots and the case for a high-viscosity lower mantle. In: Sabadini R, Lambeck K (eds.), *Glacial Isostasy, Sea-Level and Mantle Rheology*, Kluwer Academic Publishers, Norwell MA, 571–588
- Riedel MR, Karato Si (1997) Grain-size evolution in subducted oceanic lithosphere associated with the olivine-spinel transformation and its effects on rheology. *Earth Planet Sci Lett* 148:27–43
- Royden LH, Husson L (2006) Trench motion, slab geometry and viscous stresses in subduction systems. *Geophys J Int* 167:881–905
- Russo RM, Silver PG (1994) Trench-parallel flow beneath the Nazca plate from seismic anisotropy. *Science* 263:1105–1111
- Schellart WP (2004a) Kinematics of subduction and subduction-induced flow in the upper mantle. *J Geophys Res* 109, doi:10.1029/2004JB002970
- Schellart WP (2004b) Quantifying the net slab pull force as a driving mechanism for plate tectonics. *Geophys Res Lett* 31, 5
- Schellart WP, Freeman J, Stegman DR, Moresi LN (2007) Evolution and diversity of subduction zones controlled by slab width. *Nature* 446:308–311
- Schmeling H, Babeyko A, Enns A, Faccenna C, Funiciello F, Gerya T, Golabek G, Grigull S, Kaus BJP, Morra G, van Hunen J (2007) A benchmark comparison of subduction models. *Phys Earth Planet Inter* submitted
- Sdrolias M, Müller RD (2006) Controls on back-arc basin formation. *Geochemistry Geophysics Geosystems* 7, doi:10.1029/2005GC001090
- Sella GF, Dixon TH, Mao A (2002) REVEL: A model for recent plate velocities from space geodesy. *J Geophys Res* 107, doi:10.1029/2000JB000033
- Shemenda AI (1994) *Subduction: Insights from Physical Modelling. Modern Approaches in Geophysics.* Kluwer Academic Publishers, Dordrecht
- Solomon SC, Sleep NH (1974) Some simple physical models for absolute plate motions. *J Geophys Res* 79:2557–2567
- Spence W (1977) Aleutian arc - tectonic blocks, episodic subduction, strain diffusion, and magma generation. *J Geophys Res* 82:213–230
- Stegman DR, Freeman J, Schellart WP, Moresi L, May D (2006) Influence of trench width on subduction hinge retreat rates in 3-D models of slab rollback. *Geochemistry Geophysics Geosystems* 7, doi:10.1029/2005GC001056
- Stein C, Schmalz J, Hansen U (2004) The effect of rheological parameters on plate behaviour in a self-consistent model of mantle convection. *Phys Earth Planet Inter* 142:225–255
- Steinberger B (2000) Slabs in the lower mantle – results of dynamic modelling compared with tomographic images and the geoid. *Phys Earth Planet Inter* 118:241–257
- Steinberger B, Schmeling H, Marquart G (2001) Large-scale lithospheric stress field and topography induced by global mantle circulation. *Earth Planet Sci Lett* 186:75–91

- Steinberger B, Sutherland R, O'Connell RJ (2004) Prediction of Emperor-Hawaii seamount locations from a revised model of global plate motion and mantle flow. *Nature* 430:167–173
- Stevenson DJ, Turner JS (1972) Angle of subduction. *Nature* 270:334–336
- Tackley PJ (2000a) The quest for self-consistent incorporation of plate tectonics in mantle convection. In: Richards M, Gordon R, van der Hilst RD (eds.), *The History and Dynamics of Global Plate Motions*, American Geophysical Union, Washington, DC, vol. 121 of *Geophysical Monograph*
- Tackley PJ (2000b) Self-consistent generation of tectonic plates in time-dependent, three-dimensional mantle convection simulations 1. Pseudoplastic yielding. *Geochemistry Geophysics Geosystems* 1, 2000GC000036
- Tackley PJ (2000c) Self-consistent generation of tectonic plates in time-dependent, three-dimensional mantle convection simulations 2. Strain weakening and asthenosphere. *Geochemistry Geophysics Geosystems* 1, 2000GC000043
- Tackley PJ, Stevenson DJ, Glatzmaier GA, Schubert G (1994) Effects of multiple phase transitions in a three-dimensional spherical model of convection in Earth's mantle. *J Geophys Res* 99:15877–15901
- Tan E, Choi E, Thoutireddy P, Gurnis M, Aivazis M (2006) GeoFramework: Coupling multiple models of mantle convection within a computational framework. *Geochemistry Geophysics Geosystems* 7, doi:10.1029/2005GC001155
- Tan E, Gurnis M, Han L (2002) Slabs in the lower mantle and their modulation of plume formation. *Geochemistry Geophysics Geosystems* 3, 2001GC000238
- Tao WC, O'Connell RJ (1993) Deformation of a weak subducted slab and variation of seismicity with depth. *Nature* 361:626–628
- Tarduno JA, Duncan RA, Scholl DW, Cottrell RD, Steinberger B, Thordarson T, Kerr B. C. and Neal CR, Frey FA, Torii M, Carvallo C (2003) The Emperor Seamounts: Southward motion of the Hawaiian hotspot plume in Earth's mantle. *Science* 301:1064–1069
- Tetzlaff M, Schmeling H (2000) The influence of olivine metastability on deep subduction of oceanic lithosphere. *Phys Earth Planet Inter* 120:29–38
- Thoraval C, Richards MA (1997) The geoid constraint in global geodynamics: viscosity structure, mantle heterogeneity models and boundary conditions. *Geophys J Int* 131:1–8
- Toth J, Gurnis M (1998) Dynamics of subduction initiation at pre-existing fault zones. *J Geophys Res* 103:18053–18067
- Turcotte DL, Oxburgh ER (1967) Finite amplitude convective cells and continental drift. *J Fluid Mech* 28:29–42
- Turcotte DL, Schubert G (2002) *Geodynamics*. Cambridge University Press, Cambridge, 2nd edn.
- Uyeda S, Kanamori HJ (1979) Back-arc opening and the mode of subduction. *J Geophys Res* 84:1049–1061
- van der Hilst RD, Seno T (1993) Effects of relative plate motion on the deep structure and penetration depth of slabs below the Izu-Bonin and Mariana island arcs. *Earth Planet Sci Lett* 120:395–407
- van Hunen J, van den Berg AP (2007) Plate tectonics on the early Earth: limitations imposed by strength and buoyancy of subducted lithosphere. *Lithos* in press
- van Hunen J, van den Berg AP, Vlaar NJ (2000) A thermomechanical model of horizontal subduction below an overriding plate. *Earth Planet Sci Lett* 182:157–169
- van Keken PE (2003) The structure and dynamics of the mantle wedge. *Earth Planet Sci Lett* 215:323–338
- Vassiliou MS, Hager BH (1988) Subduction zone earthquakes and stress in slabs. *Pure Appl Geophys* 128:547–624
- Weijermars R, Schmeling H (1986) Scaling of Newtonian and non-Newtonian fluid dynamics without inertia for quantitative modelling of rock flow due to gravity (including the concept of rheological similarity). *Phys Earth Planet Inter* 43:316–330
- Wen L, Anderson DL (1997) Present-day plate motion constraint on mantle rheology and convection. *J Geophys Res* 102:24639–24653
- Wessel P, Smith WHF (1991) Free software helps map and display data. *EOS Trans AGU* 72:445–446
- Widiyantoro S, van der Hilst RD (1997) Mantle structure beneath Indonesia inferred from high-resolution tomographic imaging. *Geophys J Int* 130:167–182

- Wilson JT (1973) Mantle plumes and plate motions. *Tectonophysics* 19:149–164
- Yoshida M, Honda S, Kido M, Iwase Y (2001) Numerical simulation for the prediction of the plate motions: effects of lateral viscosity variations in the lithosphere. *Earth Planets Space* 53:709–721
- Zhang S, Christensen U (1993) Some effects of lateral viscosity variations on geoid and surface velocities induced by density anomalies in the mantle. *Geophys J Int* 114:531–547
- Zhong S (2001) Role of ocean-continent contrast and continental keels on plate motion, net rotation of lithosphere, and the geoid. *J Geophys Res* 106:703–712
- Zhong S, Davies GF (1999) Effects of plate and slab viscosities on geoid. *Earth Planet Sci Lett* 170:487–496
- Zhong S, Gurnis M (1994) Controls on trench topography from dynamic models of subducted slabs. *J Geophys Res* 99:15683–15695
- Zhong S, Gurnis M (1995) Mantle convection with plates and mobile, faulted plate margins. *Science* 267:838–842
- Zhong S, Gurnis M (1996) Interaction of weak faults and non-newtonian rheology produces plate tectonics in a 3D model of mantle flow. *Nature* 383:245–247
- Zhong S, Gurnis M, Moresi L (1998) Role of faults, non-linear rheology, and viscosity structure in generating plates from instantaneous mantle flow models. *J Geophys Res* 103:15255–15268
- Zhong S, Zhang N, Li ZX, Roberts JH (2007) Supercontinent cycles, true polar wander, and very long wavelength mantle convection. *Earth Planet Sci Lett* 261:551–564
- Zhong S, Zuber MT, Moresi L, Gurnis M (2000) Role of temperature-dependent viscosity and surface plates in spherical shell models of mantle convection. *J Geophys Res* 105:11063–11082